

**POLITECNICO DI TORINO**

**MASTER's Degree in Mechanical engineering**



**MASTER's Degree Thesis**

**Sideslip angle identification for tyres  
performance development**

**Supervisors**

**Prof. Enrico GALVAGNO**

**Prof. Alessandro VIGLIANI**

**Candidate**

**Andrea TORDI**

**YEAR 2020**



*To my family.*



# Acknowledgements

This research project has been performed at Balocco, FCA proving ground. I would like to start by thanking my supervisors Prof. Enrico Galvagno for giving me the possibility to complete my master's degree and for helping me to grow from a technical and personal point of view. It has been a pleasure to be mentored by him and I will always be thankful for his guidance. I am grateful to Prof. Alessandro Vigliani who accepted to be part of this project and helped me during this period.

A special thanks goes to the colleagues of Balocco, especially my tutor Eng. Alessandro Peyrot and Eng. Matteo Sacchi, who have given me the possibility to discover an awesome world, such as Balocco and have helped me with many of the decisions I have made during this period.

A very special thanks goes to my mother Silvana, my father Gino, my brother Alessandro and all the rest of my family who have supported me through this journey, without any doubt, keeping me pushing in the right direction. Since the beginning you have always trusted me even in the toughest situations, I will never forget it. Last but not least, I would like to thank my grandparents, who every day were more nervous than me for my challenges. I will never forget all that you have done for me and I can only try to give you back all the love you have given to me.

# Summary

The goal of this thesis, was to compute some parameters of dynamic vehicle such as sideslip angle and cornering stiffnesses for tyres testing, applying a linear Kalman filter, using as acquisition system either the CAN network or an IMU (Inertial measurement unit) platform. Indeed, this method works obtaining data in either cases from the CAN system and from the IMU. In testing phase, more than the sideslip angle value itself, the gap between different tyres is analysed. Indeed this work is focused especially in the tyres performance comparison.

In the first part of the thesis, some general theory topics of vehicle dynamic were treated particularly about sideslip angle estimation. A general explanation of vehicle models, specifically for the bicycle model will be done, the model picked for the sideslip angle estimation. The Kalman filter will be explained, first generally then a comparison trough different types of Kalman filters will be done; the linear Kalman filter, the EKF (Extended Kalman filter) and the UKF (Unscented Kalman filter). All the sensors used and the approach picked will be explained in detail. Furthermore a brief introduction of the code and the steps followed will be described.

In the second part, the analysis of the car behaviour for different standard manoeuvres will be showed. The manoeuvres will cover the static and dynamic behaviours of the car, in time-domain and in frequency-domain. These analysis have been done using FCA software, developed by the Fiat Research Center. The cornering stiffness estimation method will be explained. This method is based on a kinematic model, used to estimate the sideslip angle as a first estimation then to estimate the cornering stiffness.

The last point and most important aspect of this thesis, is the comparison between the results, obtained from the estimations and the measured values. The measured sideslip angle values are computed using an optical sensor and the goal of this thesis is to avoid the use of this sensor for economic and practicality reasons. These comparisons will be done for the standard manoeuvres and for the standard lap, for different types of cars, either ICE (Internal combustion engine) and Hybrid cars. At the end, a comparison between tyres performance estimation will be done, showing the model accuracy in terms of sideslip angle gap.



# Table of Contents

<b>List of Figures</b>	IX
<b>1 Introduction</b>	1
1.1 Motivation . . . . .	1
1.2 General principles . . . . .	3
1.3 Literature review . . . . .	5
<b>2 Vehicle modelling theory</b>	6
2.1 Physical quantities introduction . . . . .	6
2.2 Kinematic model . . . . .	8
2.3 Single track model . . . . .	10
2.4 Time discretization of the model . . . . .	13
2.4.1 Kinematic model discretization . . . . .	13
2.4.2 Dynamic model discretization . . . . .	14
2.5 Tyre model . . . . .	15
2.6 Pacejka . . . . .	17
2.7 Dugoff tyre model . . . . .	19
<b>3 Kalman Filter</b>	22
3.1 Filter description . . . . .	22
3.2 Principle of operation . . . . .	24
3.3 Filter application to the vehicle model . . . . .	29
3.3.1 Filter in the kinematic model . . . . .	29
3.3.2 Filter in the dynamic model . . . . .	29
<b>4 Testing and instrumentation procedure</b>	32
4.1 Balocco proving ground . . . . .	32
4.2 Manoeuvres description . . . . .	34
4.2.1 Sinusoidal steering wheel cycles (ISO 7401) . . . . .	36
4.2.2 Sweep steering wheel input (ISO7401) . . . . .	37
4.2.3 Step steering input tests (ISO 7401) and steering wheel release	38

4.2.4	Slow increasing steer . . . . .	39
4.3	Instruments . . . . .	40
4.3.1	IMU . . . . .	40
4.3.2	Optical sensor . . . . .	41
4.3.3	Universal measurement steering wheels . . . . .	42
4.4	Data Acquisition and Signal Processing . . . . .	43
4.4.1	Typical operations performed on the signals . . . . .	44
4.4.2	Command <i>lsqcurvefit</i> . . . . .	46
<b>5</b>	<b>Handling experimental analysis</b>	<b>48</b>
5.1	Introduction . . . . .	48
5.2	Tyres comparison . . . . .	49
5.2.1	Steady state behaviour analysis . . . . .	50
5.2.2	Transient behaviour analysis . . . . .	53
5.2.3	Conclusion . . . . .	62
<b>6</b>	<b>Sideslip angle estimation</b>	<b>63</b>
6.1	Introduction . . . . .	63
6.2	Structure definition . . . . .	66
6.3	First method . . . . .	69
6.4	Second method . . . . .	71
6.5	Third method . . . . .	74
6.5.1	Cornering stiffness estimation procedure . . . . .	74
6.5.2	Application . . . . .	78
6.6	Error . . . . .	82
6.7	Sideslip angle gap comparison . . . . .	84
<b>7</b>	<b>Conclusion and Outlook</b>	<b>85</b>

# List of Figures

1.1	General layout of an ANN for vehicle sideslip angle (VSA) estimation	3
1.2	Cycle modeling	4
2.1	Representation of a 4-wheel car model	7
2.2	Kinematic sideslip angle	8
2.3	Single track model	10
2.4	Tyre system	15
2.5	Lateral load Vs. slip angle	16
2.6	Cornering stiffness approximation	17
2.7	First order transfer function with $d=0.05$ m and $u=27.78$ m/s	18
2.8	Magic formula graphical representation	19
2.9	Lateral tyre force calculated by Dugoff and MF model	20
3.1	Kalman filters transformation	23
3.2	Filter scheme	26
3.3	Operation of the Kalman filter	28
3.4	Kalman filter in Simulink	31
4.1	FCA Balocco Proving Ground	33
4.2	FCA Balocco Proving Ground layout	34
4.3	ISO standard manoeuvres	35
4.4	Sinusoidal steering wheel cycles with $u = 60\text{km/h}$ $a_y = 0.25g$	36
4.5	Sweep steering wheel input with $u = 120$ km/h $a_y = 0.7g$	37
4.6	Slow increasing steer $u=100\text{km/h}$	38
4.7	Slow increasing steer $u=100\text{km/h}$	39
4.8	Example of an imu (Kistler)	40
4.9	Example of an optical sensor (Kistler) used for vehicle dynamics testing	41
4.10	Example of an universal measurement steering wheel used for vehicle dynamics testing	43

4.11	Comparison between $a_y$ , Steering angle and Yaw Rate measured by CAN and by external sensors . . . . .	44
4.12	showing tyres VSA angle and the typical optical sensor position for tests . . . . .	45
5.1	Example of vehicle data comparison . . . . .	49
5.2	Understeering curve . . . . .	50
5.3	Gradient understeering curve . . . . .	51
5.4	Sideslip angle . . . . .	51
5.5	Gradient sideslip angle . . . . .	52
5.6	Front cornering stiffness . . . . .	53
5.7	Rear cornering stiffness . . . . .	53
5.8	Bode plot between Yaw rate and steering wheel angle in a sweep frequency manoeuvre at 0.3g lateral acceleration . . . . .	55
5.9	Bode plot between Lateral acceleration and steering wheel angle in a sweep frequency manoeuvre at 0.3g lateral acceleration . . . . .	56
5.10	Bode plot between Yaw rate and lateral acceleration in a sweep frequency manoeuvre at 0.3g lateral acceleration . . . . .	57
5.11	Bode plot between Sideslip angle and Steering wheel angle in a sweep frequency manoeuvre at 0.3g lateral acceleration . . . . .	58
5.12	Bode plot between Yaw rate and steering wheel angle in a sweep frequency manoeuvre at 0.5g lateral acceleration . . . . .	59
5.13	Bode plot between Lateral acceleration and steering wheel angle in a sweep frequencies manoeuvre at 0.5g lateral acceleration . . . . .	60
5.14	Bode plot between Yaw rate and lateral acceleration in a sweep frequency manoeuvre at 0.5g lateral acceleration . . . . .	61
5.15	Bode plot between Sideslip angle and Steering wheel angle in a sweep frequency manoeuvre at 0.5g lateral acceleration . . . . .	62
6.1	Wheels speed . . . . .	64
6.2	Vehicle speed estimation and measurement . . . . .	65
6.3	Simulink block Steady state reference manoeuvre with constant cornering stiffnesses . . . . .	67
6.4	Simulink block Steady state reference manoeuvre with three values of cornering stiffnesses depending on the lateral acceleration . . . . .	68
6.5	Simulink block Steady state reference manoeuvre with two functions of cornering stiffnesses . . . . .	68
6.6	Steering angle . . . . .	69
6.7	Lateral acceleration . . . . .	70
6.8	Yaw rate . . . . .	70
6.9	Sideslip angle estimation . . . . .	71

6.10	Steering angle . . . . .	71
6.11	Lateral acceleration . . . . .	72
6.12	Yaw rate . . . . .	72
6.13	Sideslip angle estimation . . . . .	73
6.14	Simulink block cornering stiffnesses estimation . . . . .	74
6.15	Sideslip angle estimation by kinematic model . . . . .	75
6.16	Front slip angle estimation . . . . .	76
6.17	Rear slip angle estimation . . . . .	76
6.18	Front and rear forces interpolation . . . . .	77
6.19	Front and rear cornering stiffnesses estimation . . . . .	78
6.20	Sideslip angle estimation in steady state reference manoeuvre . . . . .	79
6.21	Steering angle in sweep frequency manoeuvre . . . . .	79
6.22	Lateral acceleration in sweep frequency manoeuvre . . . . .	80
6.23	Yaw rate in sweep frequency manoeuvre . . . . .	80
6.24	Bode diagram Sideslip angle estimation . . . . .	81
6.25	Sideslip angle estimation in a lap at 60 km/h . . . . .	81
6.26	Sideslip angle comparison between supplier 1,2 and 3 . . . . .	84



# Chapter 1

## Introduction

### 1.1 Motivation

Vehicle sideslip angle estimation has been a challenging task since the introduction of active systems, such as the ESC (Electronic stability control). Nowadays, vehicle control systems (VSC) enhances vehicle safe and comfort together with good environmental protection. Most Universities, research centres and companies are pushing technology's boundaries further to produce cars, safer and more ecological. The most important reason behind this continuous development is the need to increase the road safety and car accidents. In this case, they improve drivability and stability, especially assisting the driver in emergency conditions. Indeed, in these situations the loss of control can happen very quickly due to tyre saturation range.

The human being reactivity, in terms of decision-making and time to make that decision, is highly depending on the individual itself and often it is impossible for him/her to manage critical states. Therefore it is important to intervene faster and in the right way. Vehicle control systems are based on vehicle state estimation through an inertial measurement unit (IMU). An inertial measurement unit is a device that directly measures a vehicle's three linear acceleration components and three rotational rate components (and thus its six degrees of freedom). In terms of stability conditions, the most important parameter is the sideslip angle, that is defined as the angle between the vehicle's longitudinal axis and the direction of travel, taking the center of gravity as reference. Indeed a fast and accurate estimation of this parameter might help to avoid or to reduce dangerous events. The sideslip angle direct measurement requires expensive sensors such as the optical sensor, not available in standard cars. This sensor is, usually, considered a research and development tool and often forbidden in racing cars. Indeed, an estimation is usually used to overcome at this problem.

Moreover, in car testing phase, sideslip angle measurement is an important parameter to compare cars performance in terms of stability. Hence, large investments are made by the companies to have measurements as much accurate as possible and to have available an acceptable approximation of the angle. Indeed, the sideslip angle might be an indicative parameter comparing different tyres performance, especially in steady state analysis.

In the literature several methods are available, none of them can be considered the most accurate and the most profitable. The sideslip angle depends on several factor, indeed an accurate estimation is hard to obtain especially in wide working-field.

Two macro-categories of sideslip angle estimation have been identified:[1]

- **Observer-based:** This approach uses a vehicle reference model for state estimators. The results strongly depend on the model complexity, indeed it must be reached a compromise between complexity and computational burden. Moreover, at high lateral accelerations, the vehicle behaviour is usually non-linear then a complex non-linear model might be used, that leads to a higher computational cost. The most challenging tasks are usually the interaction between tyres and road surface, due to the several parameters that govern tyre behaviour, especially for the possible changes in the road conditions. Under this point of view, tyre characteristics depend on various factors like road surface conditions, temperature, tyre wear. Moreover, the observer-based might be useful in tyre testing and in vehicle development due to its flexibility. In the literature several types of observers exist, Kalman Filter (KF), with all its variants, is the most common. A GPS (Global Position System) technology can be added, to improve observed-based estimation, correcting the calculations with the receiver position. However, GPS exhibits issues such as momentary signal unavailability due to obstacles in the surrounding.
- **Neural network-based:** using this method a deep vehicle knowledge and a vehicle model is not needed. Nowadays, Artificial Neural Networks (ANN), are widely used in any field, such as vehicle control, trajectory prediction, process control and natural resource management. Artificial neural networks (ANN) are computing systems vaguely inspired by the biological neural networks, they can estimate parameters or recognize images without any prior knowledge. Artificial neural networks (ANN) are largely considered effective tools for system modelling, as they are suitable to model complex systems using their ability to identify relationships from input–output data pairs. They also offer decisive advantages such as adaptive learning, fault tolerance, and generalisation.

Moreover, in recent years, the development of high speed computers encouraged the application of ANN, which has progressed very quickly. "Using an ANN, the

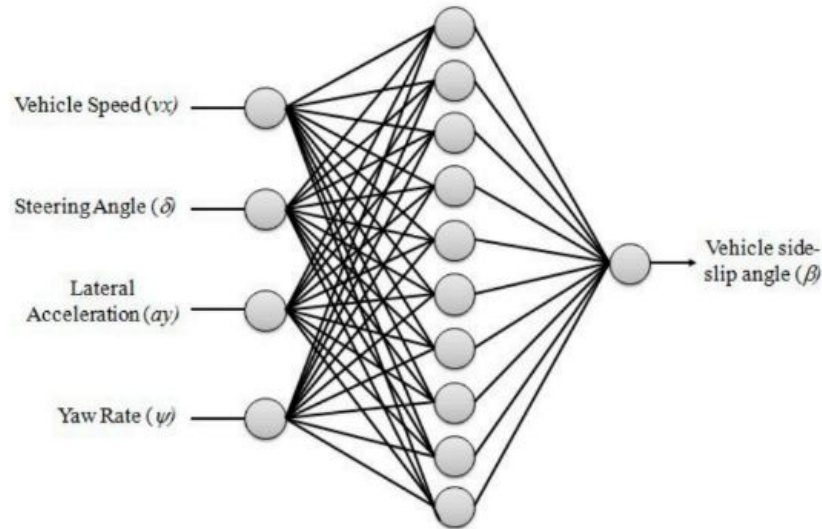


**Figure 1.1:** General layout of an ANN for vehicle sideslip angle (VSA) estimation

vehicle can be considered as a black box system, and only a conventional set of sensors is needed to train/feed the network." [1] In this case, the inputs for the black box are the yaw rate, lateral acceleration, steering angle, and vehicle speed, while the VSA is the output. Estimation results are accurate as much as the training dataset contains the whole possible scenario that the system might have to deal with. [2] However this method has a hard issue to overcome, every time the system changes, the ANN must be changed, re-performing the training procedure. The observer-based seems to be preferred in car testing phase, however the ANN might be useful when the vehicle development is made.

## 1.2 General principles

The mathematical model is a tool, that through functions and equations, describes a real event and it permits to create a connection between the inputs (physical quantities known) and outputs (unknown).

This first step of the analysis should bring to the determination of the essential aspects of the phenomenon. Furthermore if the analysis of experimental data and the assumption taken bring to a evident relation through the quantities that are essential to describe the phenomenon, then it is possible to identify the independent and dependent variables, which intervene in the phenomenon, and try to find a functional relation.

Obviously a mathematical model will never be able to describe perfectly the

real life, indeed assumptions must be taken to obtain a model mathematically describable. Moreover, if all the parameters, that have impact on the phenomenon, were taken into account, the model would be too complex and the computational cost would be too high. With the knowledge acquired on the trend of the phenomenon, it is possible to obtain functions or equations that correlate the different variables. However if there is no physical knowledge about the phenomenon a good number of experimental data are needed to have a graphical representation of it and then try to obtain a correlation of the phenomenon. A graphic representation might help to find out which mathematical formula is better to describe the phenomenon. Once the model is formulated, it is necessary to apply mathematical theories and techniques capable of solving functions or equations that govern the model to obtain information on the phenomenon, to interpret this information in a physical-experimental key, also making predictions on the future trend of the phenomenon.

A further step is to check if the mathematical model differs too much from the experimental data; if it does, the mathematical model must be changed and a new cycle start. The mathematical model should help to better understand the phenomenon and to obtain forecasts of its behaviour. A mathematical model simplifies reality "sufficiently", but, within the limits of validity of the model, that is, those imposed by the necessary simplifications, it is extremely accurate in the description and in the future forecasts on the phenomenon under examination.

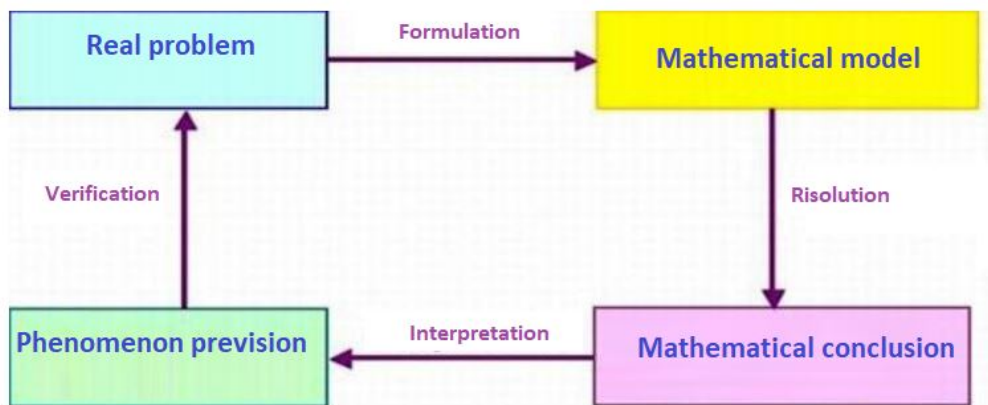


**Figure 1.2:** Cycle modeling

### 1.3 Literature review

In the literature several types of models are developed to estimate the sideslip angle, Wang et al.[3] use a closed-loop state feedback observer based on IMU measurements, longitudinal velocity and an inverted Dugoff tyre model.[4] Grip et al.[5] use a non-linear observer based on asymptotic stabilisation of estimation errors. Other approaches are those of Shraim et al.[6] and Cadiou et al.[7] who use sliding mode observers and Zhao et al.[8] who use moving horizon strategies. So far, all the models use a combination of vehicle model and a tyre model to obtain lowest error. Although modelling errors cannot be completely eliminated with model-based observers, estimation can still be improved with adaptive methods. Zhang et al.[9] use a gain-scheduling observer based on a linear parameter-varying system while You et al.[10] use online adaptive laws based on yaw rate dynamics and lateral acceleration measurements.

The most common method to estimate the sideslip angle, based on vehicle dynamics models, is the Kalman Filter (KF) and its derivations. There are several types of Kalman filters and most of them are applied to vehicle models. Ryu et al.[11] apply the linear Kalman filter to a lateral dynamics model, based on of combination of GPS and IMU measurements. Doumiati et al.[12] applied an Extended Kalman Filter (EKF) directly to a simplified vehicle model, considering the road friction known, using a Dugoff tyre model. The best description of tyre dynamics is by Huang et al.[13] and Li et al.[14] who use the standard Pacejka tyre model.[15] Hodgson et al.[16] also use the Pacejka tyre model, however, they adapt the tyre force curve in real-time by using a simplified vehicle model. Baffet et al.[17] use a Sliding Mode Observer (SMO) while Lian et al.[18] calculate cornering stiffness with a Recursive Least Squares (RLS) regression model. These forces are then used in a simplified vehicle model and an EKF is applied to estimate the sideslip angle. Many other methods to estimate tyre forces exist. For Julier et al.[19] the EKF is only reliable for systems which are almost linear within the operating frequency range. This would make it necessary to operate at very high frequency when tyres are in the saturation region to assure linearity, which is, however, not feasible with a normal production Electronic Control Unit (ECU).[20]

# Chapter 2

## Vehicle modelling theory

### 2.1 Physical quantities introduction

"As vehicles are becoming more and more performing throughout the years, it turns out that their design process requires better knowledge of their behaviour. One of the ways to get to that knowledge is to use mathematical models, which describe the behaviour of the vehicle when given relevant parameters. Knowing these parameters is essential to run the models, and get the expected results." [21] In the literature there are several types of algorithms to estimate the sideslip angle, here below all the physical quantities available to compute it, will be explained.

All the important physical quantities in vehicle dynamics used in the algorithms to estimate the beta angle:

- $\delta_v$ : Steer angle
- $u_n$ : Longitudinal velocity
- $a_y$ : Lateral acceleration
- $a_x$ : Longitudinal acceleration
- $\dot{\psi}$ : Yaw rate
- $\dot{\vartheta}$ : Roll rate
- $\dot{\phi}$ : Pitch rate

In terms of vehicle dynamic an important parameter, used to determine the stability of a car, is the sideslip angle, also called beta angle. This angle represents the angle between the vehicle's longitudinal axis and the direction of travel. This angle might be computed in every point of the car however at the end it is usually represented at the center of gravity of the vehicle. The sideslip angle is very useful



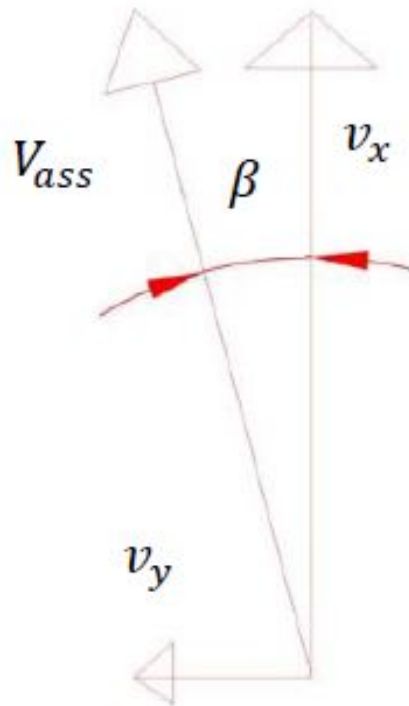


Figure 2.2: Kinematic sideslip angle

## 2.2 Kinematic model

The idea behind the kinematic model is, to define vehicle model similar to "real" one, with the substantial difference that the vehicle is considered as a rigid body, avoiding to take into account all the dynamic theory part.

In a translation, all the points of the vehicle, that is considered a rigid body, describe a common trajectory with the same speed as the center of gravity. While in a rotation, all the points have the same rotational speed  $\omega$ , however the speeds  $V_i$  are different and they depend on the distance from the rotation-axis.

It requires strong hypotheses, indeed it represents correctly the vehicle behaviour only in some circumstances. However it might be useful as a first approximation as well as to compute unknown parameters in the dynamic model.

The kinematic model correlates the two components of accelerations measured in the center of gravity of the vehicle (longitudinal  $a_x$  and lateral  $a_y$ ) and the relative velocities respect to the vehicle-based reference frame. This model has only three degrees of freedom in the absolute reference frame:

1. X-coordinate
2. Y-coordinate
3. Z-rotation

By knowing the correlation between velocity and acceleration:

$$\begin{cases} v_g = u\mathbf{i} + v\mathbf{j} \\ a_g = a_x\mathbf{i} + a_y\mathbf{j} = \frac{dV_g(x)}{dt} \end{cases}$$

Therefore the system can be represented by two equations:

$$\begin{cases} a_x = \dot{u} - \dot{\psi}v \\ a_y = \dot{v} + \dot{\psi}u \end{cases}$$

with:

- $u$ : Longitudinal velocity
- $a_y$ : Lateral acceleration
- $a_x$ : Longitudinal acceleration
- $\dot{\psi}$ : Yaw rate
- $v$ : Lateral velocity

This system of equations can be represented in matrix notation:

$$\begin{pmatrix} \dot{u} \\ \dot{v} \end{pmatrix} = \begin{bmatrix} 0 & \dot{\psi} \\ -\dot{\psi} & 0 \end{bmatrix} \begin{pmatrix} u \\ v \end{pmatrix} + \begin{pmatrix} a_x \\ a_y \end{pmatrix} \quad (2.1)$$

Although this model seems so simple, it is worth especially for its simplicity. Indeed it requires just accelerations and yaw rate measurements to obtain the two velocities ( $v$  and  $u$ ) and furthermore from these two quantities it is possible to obtain the sideslip angle as it follows:

$$\beta = \arctan\left(\frac{v}{u}\right) \quad (2.2)$$

Obviously this can work just in theory, due to several reasons. The measurements are never accurate as wanted due to the noise and others external events that might change the result. Moreover, pitch and roll angles are neglected and they represent a part of the error on the estimation.



equal to  $m$ . The wheelbase is  $L$  and the length of the the distances between the center of gravity and the front and the rear wheel line are respectively  $a_1$  and  $a_2$ . The mass moment of inertia with respect to z-axis is  $I_z$  and slip angles  $\alpha_1$  and  $\alpha_2$ , are assumed to be small as well as steering angle  $\delta_1$ . Further hypothesis considered:

- The longitudinal state of the vehicle is substitute by the longitudinal speed. Indeed, the effect of the longitudinal forces on vehicle lateral dynamics is neglected;
- The angle (Rear steering angle) is null, considering only a front steering car and neglecting the effect of suspension;
- $J$  is the z moment of inertia computed at the center of gravity

The two equations that govern the dynamic system are:

$$\begin{aligned} m(\dot{v} + u\dot{\psi}) &= F_{y1} + F_{y2} \\ J\ddot{\psi} &= F_{y1}a_1 - F_{y2}a_2 \end{aligned} \quad (2.3)$$

Considering  $\delta_1$  (front steering wheel angle) small, therefore  $\cos(\delta_1) \approx 1$

Introducing the steering ratio ( $\tau$ ),  $\delta_1 = \tau\delta_v$ , the two congruence equations for the slip angles are:

$$\begin{aligned} \alpha_1 &= \tau\delta_v - \left(\frac{v + \dot{\psi}a_1}{u}\right) \\ \alpha_2 &= -\left(\frac{v - \dot{\psi}a_2}{u}\right) \end{aligned} \quad (2.4)$$

and the two linear constitutive equations:

$$\begin{aligned} F_{y1} &= C_1\alpha_1 \\ F_{y2} &= C_2\alpha_2 \end{aligned} \quad (2.5)$$

In case of manoeuvres, with small slip angles,  $\max 3 \div 4^\circ$ , the tyres linear model can be applied.

Furthermore, combining these two equations the relations below are obtained:

$$\begin{aligned} F_{y1} &= C_1\alpha_1 = C_1\left(\delta_1 - \frac{v + \dot{\psi}a_1}{u}\right) \\ F_{y2} &= C_2\alpha_2 = C_2\left(\frac{v - \dot{\psi}a_2}{u}\right) \end{aligned} \quad (2.6)$$

that link linearly the lateral forces to the state variables  $(v, \dot{\psi})$ .

Substituting these relations into the equilibrium equations:

$$\begin{aligned} m(\dot{v} + u\dot{\psi}) &= C_1\left(\delta_1 - \frac{v + \dot{\psi}a_1}{u}\right) + C_2\left(-\frac{v - \dot{\psi}a_2}{u}\right) \\ J\ddot{\psi} &= C_1a_1\left(\delta_1 - \frac{v + \dot{\psi}a_1}{u}\right) - C_2a_2\left(-\frac{v - \dot{\psi}a_2}{u}\right) \end{aligned} \quad (2.7)$$

that, in synthetic way, it can be rewritten:

$$\begin{aligned} \dot{v} &= Y_v v + Y_{\dot{\psi}} \dot{\psi} + Y_{\delta} \delta_v \\ \ddot{\psi} &= N_v v + N_{\dot{\psi}} \dot{\psi} + N_{\delta} \delta_v \end{aligned} \quad (2.8)$$

As a final step, the ultimate relation in matrix form has been obtained:

$$\dot{w} = Aw + b\delta_v \quad (2.9)$$

Where  $w(t) = (v(t), \dot{\psi}(t))^T$  represents the state vector.

with:

$$b(t) = \tau \begin{bmatrix} \frac{C_1}{m} \\ \frac{C_1 a_1}{J} \end{bmatrix} \quad (2.10)$$

and

$$A = A(t) = - \begin{bmatrix} \frac{C_1 + C_2}{mu} & \frac{C_1 a_1 - C_2 a_2}{mu} + u \\ \frac{C_1 a_1 - C_2 a_2}{Ju} & \frac{C_1 a_1^2 + C_2 a_2^2}{Ju} + u \end{bmatrix} \quad (2.11)$$

is the matrix of coefficients. It is important to notice that A depends only by the speed of the vehicle  $u$ , but not by  $\delta_v$ , that instead multiplies  $b$ .

All the parameters needed by the model:

- $C_1$ : Front cornering stiffness
- $C_2$ : Rear cornering stiffness
- $a_1$ : Front-wheel line and center of gravity distance
- $a_2$ : Rear-wheel line and center of gravity distance
- $u$ : Longitudinal speed
- $\tau$ : Steering ratio
- $J$ : Mass moment of inertia z-axis at the center of gravity
- $m$ : Mass of the vehicle

## 2.4 Time discretization of the model

### 2.4.1 Kinematic model discretization

So far, all the systems described were continuous systems. Obtaining signals as discrete points a discretization model is needed. Indeed dividing the time domain in tiny intervals, a state of the system at a right time is obtained. Applying the Euler method, that is a first-order numerical procedure for solving ordinary differential equations. The method is based on approximating the time derivative with the incremental ratio:

$$\dot{x} = \frac{dx}{dt} = \frac{x_{k+1} - x_k}{T_s}$$

With  $T_s$  the sampling time,  $x_{k+1}$  state of the system at time k+1 and  $x_k$  at time k. Taking the equations of motion from the kinematic model, the state of the system is:

$$\begin{cases} \dot{u} = \dot{\psi}v + a_x \\ \dot{v} = -\dot{\psi}u + a_y \end{cases}$$

Applying the Euler method:

$$\begin{cases} \frac{u_{k+1} - u_k}{T_s} = \dot{\psi}v + a_x \\ \frac{v_{k+1} - v_k}{T_s} = -\dot{\psi}u + a_y \end{cases}$$

Rearranging:

$$\begin{cases} u_{k+1} = u_k + T_s \dot{\psi}_k v_k + T_s a_{xk} \\ v_{k+1} = v_k - T_s \dot{\psi}_k u_k + T_s a_{yk} \end{cases}$$

Writing in matrix form:

$$\begin{pmatrix} u_{k+1} \\ v_{k+1} \end{pmatrix} = \begin{bmatrix} 1 & T_s \dot{\psi} \\ T_s - \dot{\psi} & 1 \end{bmatrix} \begin{pmatrix} u_k \\ v_k \end{pmatrix} + \begin{bmatrix} T_s & 0 \\ 0 & T_s \end{bmatrix} \begin{pmatrix} a_{xk} \\ a_{yk} \end{pmatrix} \quad (2.12)$$

Writing it in generic form, where  $x$  represents the state of the system and  $u$  the input:

$$x_{k+1} = A_k x_k + T_s B u_K \quad (2.13)$$

As we can see the matrix  $A$  changes every loop, due to the presence of the yaw rate, instead  $B$  remains constant.

## 2.4.2 Dynamic model discretization

Taking the equation of motion from the single track model, the state of the system is:

$$\begin{aligned} \dot{v} &= Y_v v + Y_{\dot{\psi}} \dot{\psi} + Y_{\delta} \delta_v \\ \ddot{\psi} &= N_v v + N_{\dot{\psi}} \dot{\psi} + N_{\delta} \delta_v \end{aligned} \quad (2.14)$$

Applying the Euler method and rearranging in matrix form:

$$\begin{pmatrix} v_{k+1} \\ \dot{\psi}_{k+1} \end{pmatrix} = \begin{bmatrix} T_s Y_v + 1 & T_s Y_{\dot{\psi}} \\ T_s N_v & N_{\dot{\psi}} T_s + 1 \end{bmatrix} \begin{pmatrix} v_k \\ \dot{\psi}_k \end{pmatrix} + \begin{pmatrix} Y_{\delta} \\ N_{\delta} \end{pmatrix} \delta_v \quad (2.15)$$

Writing it in generic form, where  $x$  represents the state of the system and  $u$  the input:

$$x_{k+1} = A_k x_k + T_s B u_K$$

As we can see, in this case, the matrix  $A$  is constant.

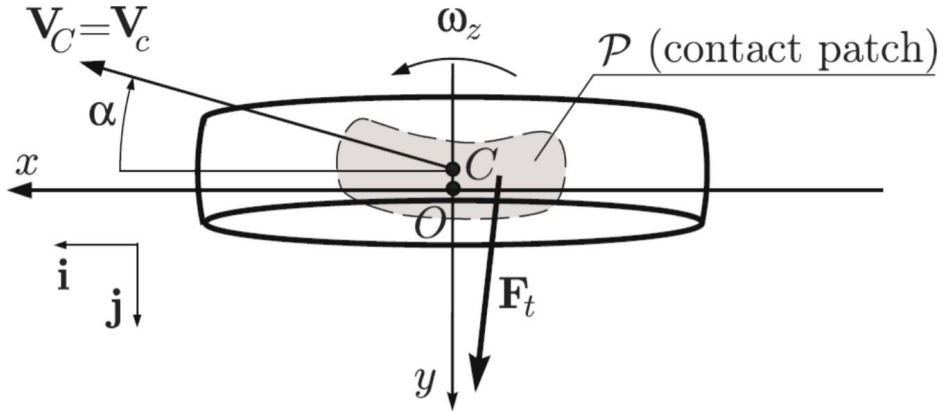


Figure 2.4: Tyre system

## 2.5 Tyre model

In Fig.2.4 is represented the tyre reference frame. The origin  $O$  is taken on the road plane and coincident with the center of the contact patch in pure rolling.

In lateral dynamic, the lateral force  $F_y$  is the most important force that the tyres exchange with the road. It is practice to show  $F_y$  behaviour respect to the slip angle as well as the vertical load.[22]

$$F_y = Y_p(\alpha, F_z, \mu, \gamma) \quad (2.16)$$

Whith:  $\gamma$  is the camber angle and  $\mu$  is the adhesion coefficient.

$Y_p$  represents the characteristic function of the tyre, obviously trying to simplify the problem, without considering all the parameters that intervene in the tyre behaviours. For tyre behaviours an important parameter is the cornering stiffness, that is equal to:

$$C_\alpha = C_\alpha(F_z) = \frac{\partial Y_p}{\partial \alpha} \quad (2.17)$$

Evaluated in  $\alpha = 0$  and  $F_z = const.$

Experimentally,  $C_\alpha$  increases less than proportional respect to the vertical load  $F_z$  (Fig.2.4).

The utility of the cornering stiffness  $C_\alpha$  is in the series expansion, indeed:

$$F_y = C_\alpha \alpha + O(\alpha^2) \quad (2.18)$$

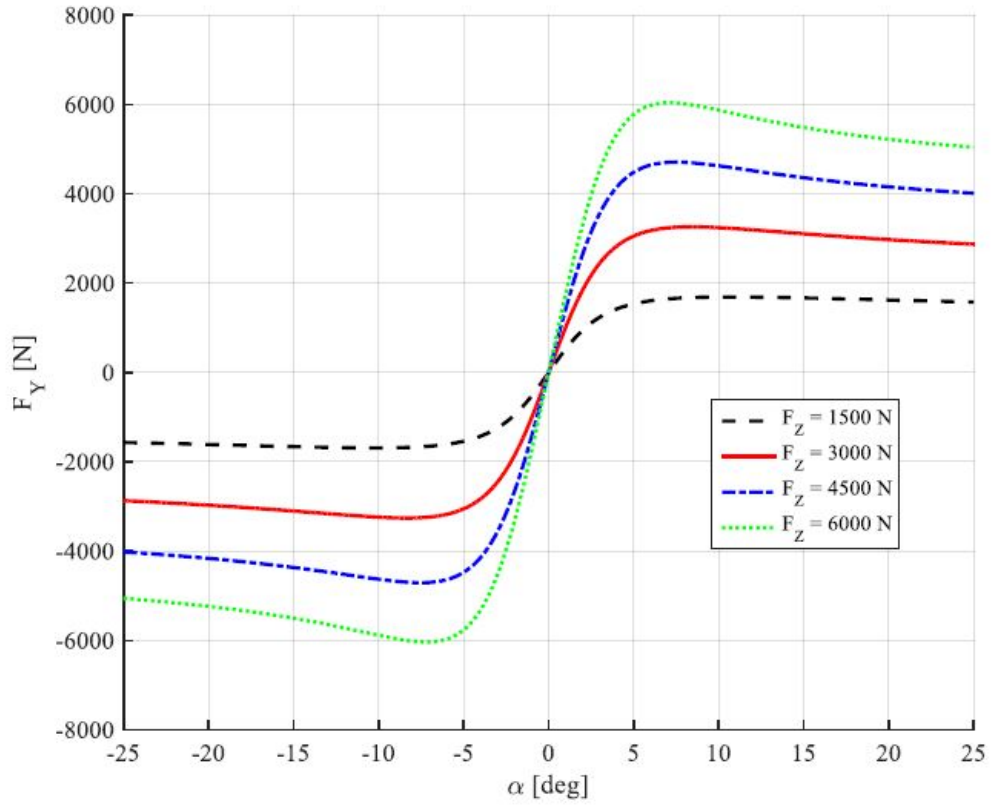


**Figure 2.5:** Lateral load Vs. slip angle

The final linear relation between the lateral forces and slip angles can be written:

$$F_y = C_\alpha \alpha \quad (2.19)$$

So far, the model assumed a real-time response of the tyre varying the slip angle. However the tyre behaviour is different, a delay is present. Keeping the linear model above (Eq.2.18) the model becomes a differential equation:

$$\frac{d}{u} \dot{F}_{yi} + F_{yi} = C_i \alpha_i(t) \quad (2.20)$$

Where  $d$  is the relaxation length of each tyre.

The first order transfer function:

$$\frac{F_{xRit}}{F_{xPac}} = \frac{1}{\tau S + 1} \quad (2.21)$$

Where  $\tau = \frac{d}{u}$

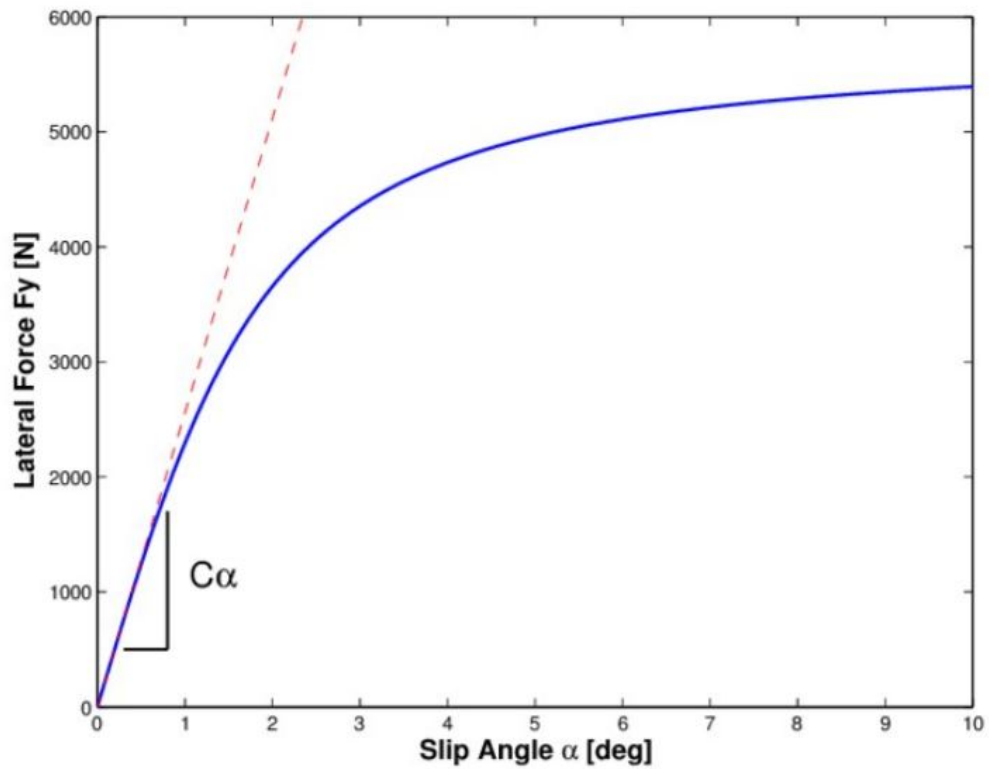


Figure 2.6: Cornering stiffness approximation

## 2.6 Pacejka

The Pacejka formulation at four coefficients (Magic formula) is the simplest one and its expression (the function of the four coefficients  $B, C, D$  and  $E$ ) is:

$$y(x) = D \sin(C \arctan(Bx - E(Bx - \arctan(Bx)))) \quad (2.22)$$

The four coefficients generally are called:

- $B$  stiffness factor
- $C$  shape factor
- $D$  peak value
- $E$  curvature factor

Furthermore this formulation has the follow hypothesis:

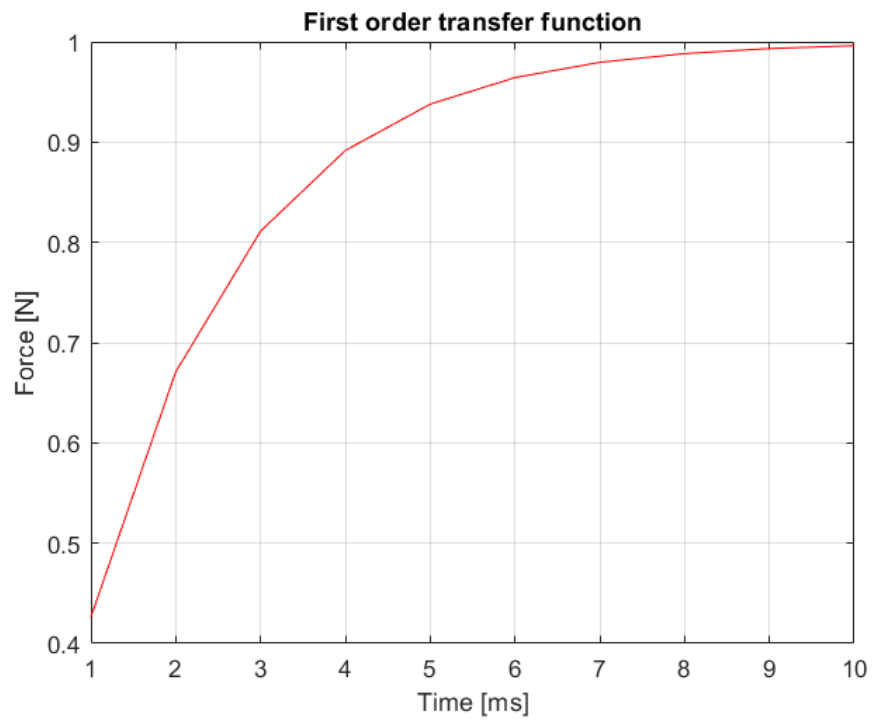


**Figure 2.7:** First order transfer function with  $d=0.05$  m and  $u=27.78$  m/s

- Upper limited  $|y| \leq D$
- The value of the derivative in zero is:  $y(0) = BCD$
- The asymptotic value is:  $y_{as} = D \sin(\frac{\pi}{2}C)$

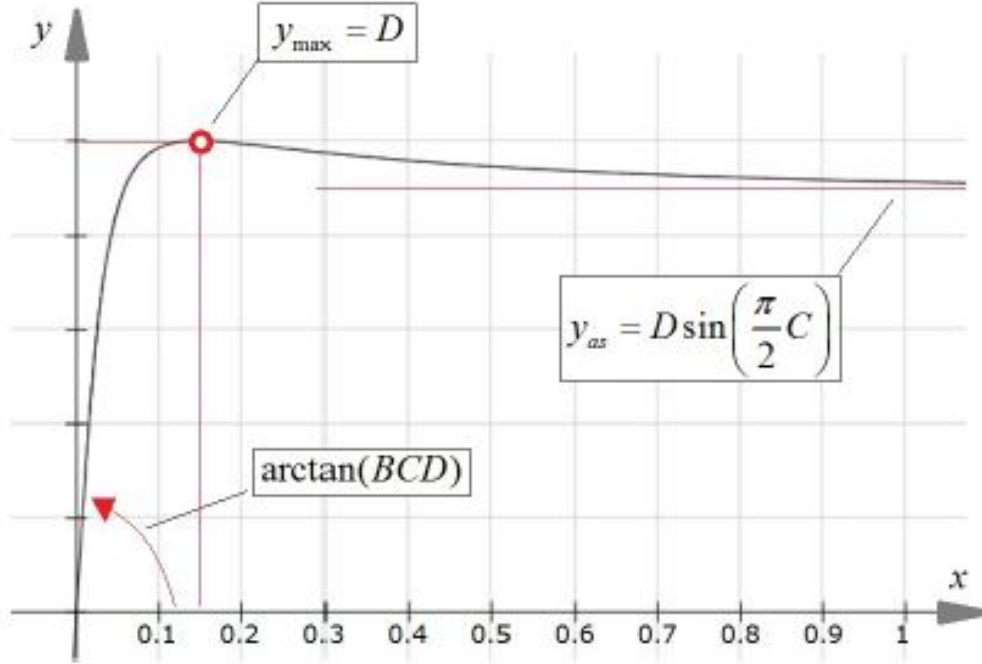


Figure 2.8: Magic formula graphical representation

## 2.7 Dugoff tyre model

With a simple form, Dugoff tyre model can calculate the longitudinal and lateral tyre force under pure longitudinal slip, pure side slip and associated longitudinal side slip situation. So it was used by lots of researchers to reach better real-time performance. Dugoff tyre model is described as:

$$F_x = C_s \frac{S}{1 + S} f(\lambda) \quad (2.23)$$

$$F_y = C_\alpha \frac{\tan \alpha}{1 + S} f(\lambda) \quad (2.24)$$

In above equations the variables are used as follows:  $F_x$  and  $F_y$  are the longitudinal and lateral forces of tyres.  $C_s$  and  $C_\alpha$  are the longitudinal and lateral stiffness of tyres.  $S$  is the longitudinal slip ratio of tyres and  $\alpha$  is the tyre sideslip angle.  $\lambda$  and the function  $f(\lambda)$  are described as:

$$\lambda = \frac{\mu_{max} F_z (1 + S)}{2\sqrt{(C_s S)^2 + (C_\alpha \tan \alpha)^2}} \quad (2.25)$$

$$f(\lambda) = \begin{cases} (2 - \lambda)\lambda, & \lambda < 1 \\ 1, & \lambda \geq 1 \end{cases}$$

Among the above formula  $F_z$  is the vertical load force of tyres;  $\mu_{max}$  is the maximum friction coefficient.

Although fit for expressing the change trend of the friction forces generated from the tyre and road interface, the precision of Dugoff model decreases a lot in condition of large wheel slip ratio or large sideslip angle when compared with Magic Formula, which is commonly considered as the accurate model for road friction illustration. The comparison of the longitudinal and lateral tyre forces calculated

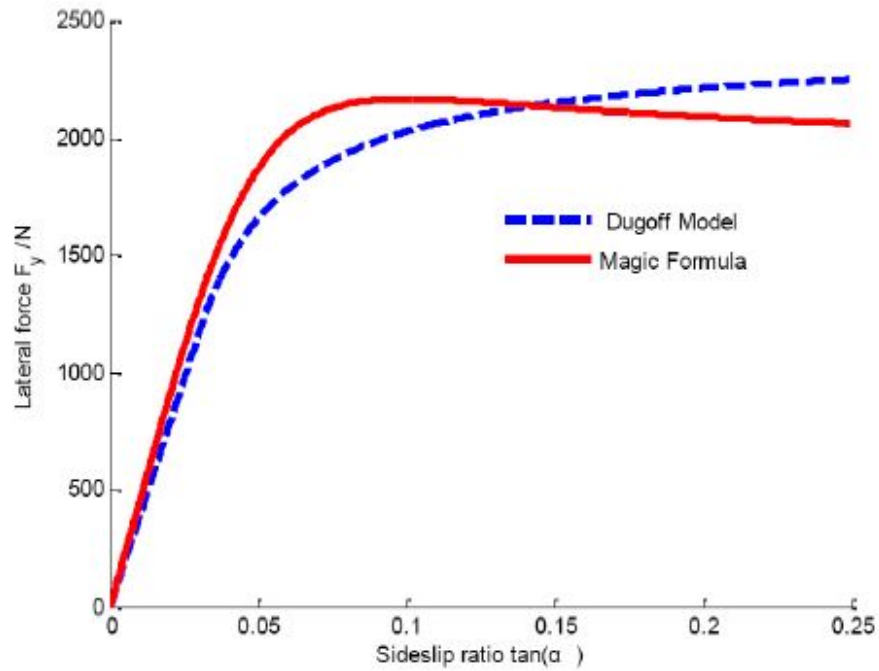


**Figure 2.9:** Lateral tyre force calculated by Dugoff and MF model

by Dugoff and MF tyre model is shown in Figure 2.9. It indicates that: there is no peak point in Dugoff model; and the difference of these two models is larger with

large slip ratios. The Dugoff model must be modified because the model precision is very important when the slip ratio is large, in such a situation a vehicle is easy to lose stability.

The reason leading to the error with large slip ratio is that the Dugoff model does not reflect the truth that the tyre friction coefficient  $\mu$  decreases when the slip ratio is enough large. For solving this problem, some modification method should be taken.[4]

# Chapter 3

## Kalman Filter

### 3.1 Filter description

The Kalman filter takes the name from its inventor R. E. Kalman, who in 1960 published his paper describing a recursive solution to the discrete-data linear filtering problem. Since that time, due in large part to advances in digital computing, the Kalman filter has been the subject of extensive research and application, particularly in the area of autonomous or assisted navigation.

"Theoretically the Kalman Filter is an estimator for what is called the linear-quadratic problem, which is the problem of estimating the instantaneous "state" of a linear dynamic system perturbed by white noise, by using measurements linearly related to the state but corrupted by white noise. The resulting estimator is statistically optimal with respect to any quadratic function of estimation error".[23]

The Kalman filter provides, from indirect measurements, an estimation for the missing information, that usually it can not be measured. The Kalman filter is also used for predicting dynamic systems behaviour, such as the trajectories of aircraft.

The Kalman filter, controlling the inputs of a system's dynamic model and multiple measurements, usually from one or more sensors, computes an estimation of the system state. The Kalman filter mixes the data obtained from the sensor and the data computed by the algorithm. Indeed a mathematical model, as accurate as possible, must represent the physical problem. Therefore, the mathematical model has an uncertainty as well as the measurement from the sensor and that uncertainties are represented by the covariance. The Kalman filter is a recursive method, in fact every step it has the new state-estimate and its new covariance. The estimation produced by the Kalman filter, is a weighted average between the system's predicted state and the current measurement, using the Kalman's gain, a parameter computed every step from the covariances at the previous step.

The application of Kalman filtering encompasses many fields, but its use as a

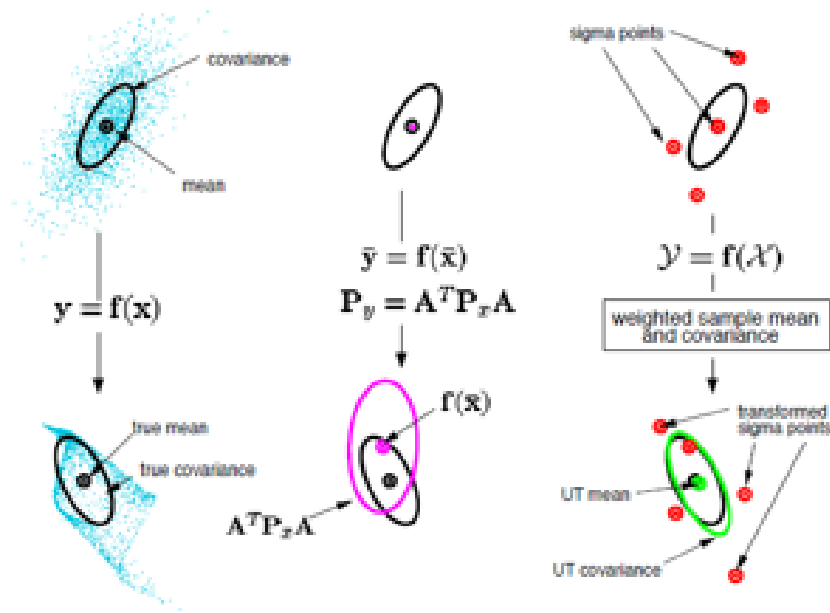


**Figure 3.1:** Kalman filters transformation

tool is almost exclusively for two purposes: *estimation and performance analysis of estimators*.

1. *Estimating the state of Dynamic Systems.* Nearly all physical systems are dynamic to some degree, except for a few fundamental physical constants. Indeed if a precise estimates, of time-dependent characteristics, is the goal, then their dynamics must be taken into consideration. The problem is that their dynamics not always is known very precisely. Kalman filter explains this ignorance using probabilities. The Kalman filter allows us to estimate the state of dynamic systems by using statistical information.
2. *The Analysis of Estimation Systems.* The objective of design analysis is to determine how best to use these type of sensors for a given set of design criteria. These criteria are typically related to estimation accuracy and system cost.

The Kalman filter determines the optimal filtering gains from the probability distribution of its estimation errors, and this probability distribution may be used in evaluating its performance as a function of the "design parameters" of an estimation system.

The linear Kalman filter is an optimal linear estimator, however it is based on the assumption that the process noise and measurement noise are Gaussian noises,

therefore with Gaussian amplitude distribution. In linear Kalman filter, only mean and covariance of the state are taken into account in its update rule. Nonlinear problems can be solved with the extended Kalman filter (EKF).

In situations, such as tyre behaviour at limit handling, the problem is non-linear and a linear Kalman filter might not be optimal, the result might be far from an acceptable one.

The extended Kalman filter is based upon the principle of linearization of the state transition matrix and the observation matrix with Taylor series expansions. Exploiting the assumption that all transformations are quasi-linear, the EKF simply makes linear all non-linear transformations and substitutes Jacobian matrices for the linear transformations in the Kalman filter equations. The linearization can lead to poor performance and divergence of the filter for highly non-linear problems. An improvement to the extended Kalman filter is the unscented Kalman filter (UKF). The UKF approximates the probability density resulting from the non-linear transformation of a random variable. It is done by evaluating the non-linear function with a minimal set of carefully chosen sample points. The posterior mean and covariance estimated from the sample points are accurate to the second order for any non-linearity.

## 3.2 Principle of operation

In reality, the output of a system is a measurement, typically affected by noise. The sensors might be inaccurate and this is represented by an input noise. The models as well, are inaccurate by definition and this can be modeled by an input noise.

The Kalman filter is an optimal observer, under some hypothesis.

Considering a dynamic linear system, not stationary and continuous:

$$\begin{cases} \dot{x}(t) &= A(t)x(t) + B_u(t)u(t) + B_w w(t) \\ y(t) &= C(t)x(t) + v(t) \end{cases}$$

with the initial state:  $x(t_0) = x_0$

where:

- $w(t)$  is the process noise
- $v(t)$  is the measurement noise
- $y(t)$  is the measurement output

It is assumed that  $w$  and  $v$  are stochastic Gaussian, stationary, white processes with null average. Furthermore,  $w(t)$  and  $v(t)$  are casual variable with Gaussian distribution.

The process and measurement noises are independent from each other:

$$E[w(t_1)v^T(t_2)] = 0, \forall t_1, t_2 \quad (3.1)$$

Moreover, the initial state is a Gaussian casual variable with average and covariance known:

$$E[x_0] = \bar{x}_0 \quad (3.2)$$

$$E[(x_0 - \bar{x}_0)(x_0 - \bar{x}_0)^T] = P_0 \quad (3.3)$$

A further assumption is, that the stochastic processes  $w(t)$  and  $v(t)$  are not correlated with  $x_0$ .

If the couples  $(A, B_w)$  and  $(A, C)$  are respectively, controllable and observable, then the observer:

$$\dot{\hat{x}}(t) = A(t)\hat{x}(t) + B_u(t)u(t) + L(t)(y(t) - C(t)\hat{x}(t)) \quad (3.4)$$

is stable and optimum, that means that minimizes the mean squared error:

$$E[e^T(t)e(t)] \quad (3.5)$$

with  $e(t) = x(t) - \hat{x}(t)$

If the gain is picked as:

$$L(t) = P(t)C^T(t)V^{-1}(t) \quad (3.6)$$

Where  $P(t)$  is the solution for the Ricatti equation.

The Kalman filter is a recursive estimator. This means that only the estimated state from the previous time step and the current measurement are needed to compute the estimate for the current state. Indeed, no history of measurements is required.

The Kalman filter is often conceptualized as two distinct phases: "Predict" and "Update". The predict phase uses the state estimate from the previous time-step to produce an estimate of the state at the current time-step.

The predicted state estimation also called a priori state estimation because it does not need information from the current time-step. The a posteriori estimation instead, uses the current observation information and the current state estimation (the a priori estimate). Moreover the a posteriori estimation will be used for the next time-step. The filter works recursively step by step on the estimation made by the model.

The Kalman filter at discrete time is used in real system, transforming continuous linear system in a discrete linear system such as:

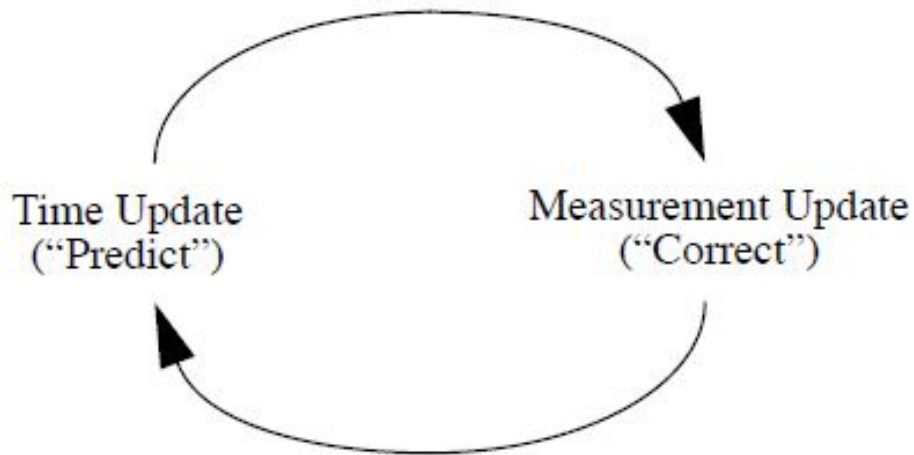


**Figure 3.2:** Filter scheme

$$\begin{cases} x_{k+1} &= A_k x_k + T_s B u_k \\ y_k &= C x_k + T_s D u_k \end{cases}$$

These equations represent the state of the system.

In addition to the state of the system, the real part of the filter must be developed, starting from the covariance matrices. The covariance matrices are three:

- $Q$ , the covariance matrix that represents the accuracy of the model. The lower the values on the diagonal are the more accurate is the mathematical model.

$$\begin{bmatrix} w_{k1} & \dots & 0 \\ \vdots & \ddots & \vdots \\ 0 & \dots & w_{kn} \end{bmatrix}$$

$w_k$  represents an estimation of the model error.

- $R$ , the covariance matrix that stands for the accuracy of the measurements. As for the model, the lower the values on the diagonal are the more accurate are the measurements.

$$\begin{bmatrix} z_{k1} & \dots & 0 \\ \vdots & \ddots & \vdots \\ 0 & \dots & z_{kn} \end{bmatrix}$$

$z_k$  represents an estimation of the measurements errors

- P, is an overall matrix that takes into account the filter estimation. It is computed as a function of Q, R and Kalman gain. The matrices R and Q are kept constant for every step, instead the P matrix is updated every time-step. Indeed, a priori and a posteriori P matrix will be calculated at every k-time. The a priori matrix will be:

$$P_k^- = A_k P_{k-1} A_k^T + Q \quad (3.7)$$

Where  $A_k$  is the matrix of the dynamic model and  $P_{k-1}$  is the covariance matrix at the previously step.

The state initiation,  $x_k(k = 1)$  contains the measurement state:

$$x_k(k = 1) = \begin{pmatrix} x_{1m} \\ \vdots \\ x_{nm} \end{pmatrix} \quad (3.8)$$

The initiation of the covariance matrix, assumes:

$$P^-(k = 1) = Q \quad (3.9)$$

Terminated the initiation phase, the a priori state of the system will be defined:

$$x_k^- = A_k x_{k-1} + T_s B u_{k-1} \quad (3.10)$$

Where  $x_k^-$  is the a priori estimation of the state, instead  $x_{k-1}$  is the a posteriori estimation at the previously time-step. The same procedure for the covariance matrix by the Eq.3.7. The formula for the updated (a posteriori) estimate covariance above is valid for the optimal ( $K_k$ ) gain that minimizes the residual error, in which form it is most widely used in applications. The principal parameter to correct the estimation is the Kalman gain ( $K_k$ ). This parameter is computed every loop and is multiplied by the correction factor. In the linear case, the Kalman gain at time-step k is given as:

$$K_k = P_k^- C^T (C P_k^- C^T + R)^{-1} \quad (3.11)$$

that will be used in the correction of the state vector estimation  $x_k^-$  given from the model:

$$x_k = x_k^- + K_k (\bar{y}_k - y_k) \quad (3.12)$$

With  $y_k = C x_k + T_s D u_k$

The parameter  $x_k$  will be the final value of the state system, considering either the theoretical model and the measurements. Once the state is computed the covariance matrix  $P_k$  will be updated:

$$P_k = [I - K_k C] P_k^- [I - K_k C]^T + K_k R K_k^T \quad (3.13)$$

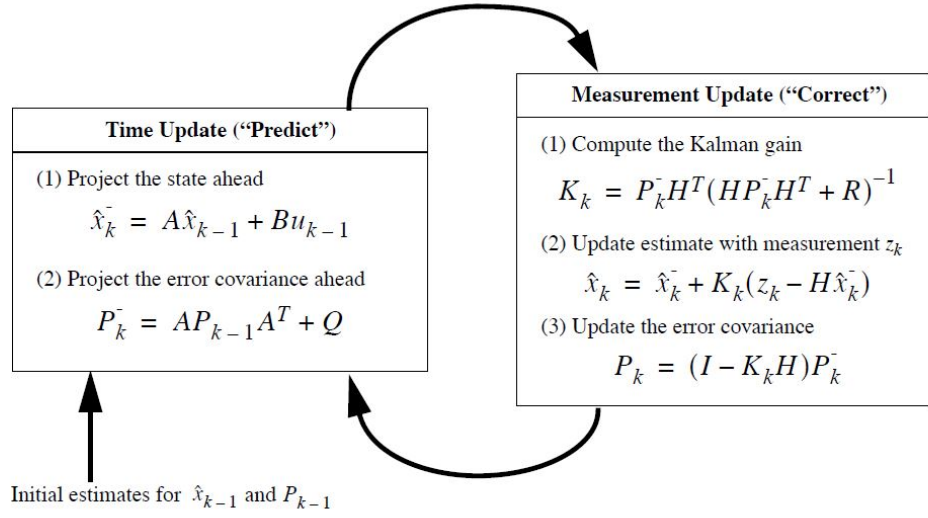


**Figure 3.3:** Operation of the Kalman filter

### 3.3 Filter application to the vehicle model

The discrete Kalman filter might be used for every linear dynamic system. In the next two paragraphs the application to the kinematic and dynamic model will be showed.

#### 3.3.1 Filter in the kinematic model

In this part the filter for the kinematic model can be summarized as:

$$\begin{pmatrix} u_{k+1} \\ v_{k+1} \end{pmatrix} = \begin{bmatrix} 1 & T_s \dot{\psi} \\ T_s - \psi & 1 \end{bmatrix} \begin{pmatrix} u_k \\ v_k \end{pmatrix} + \begin{bmatrix} T_s & 0 \\ 0 & T_s \end{bmatrix} \begin{pmatrix} a_{xk} \\ a_{yk} \end{pmatrix} \quad (3.14)$$

- Input:
  - $a_x$ , longitudinal acceleration
  - $a_y$ , lateral acceleration
- State of the system:
  - $u$ , longitudinal velocity
  - $v$ , lateral velocity
- Measurement:
  - $a_x$ , longitudinal acceleration
  - $a_y$ , lateral acceleration
  - $\dot{\psi}$ , yaw rate
  - $u$ , longitudinal velocity

Moreover, from the state computed, the longitudinal speed estimation by the model is compared with the measured one and then the state of the system is corrected as explained previously on the Kalman filter procedure.

#### 3.3.2 Filter in the dynamic model

In this part the filter for the dynamic model can be summarized as:

$$\begin{pmatrix} v_{k+1} \\ \dot{\psi}_{k+1} \end{pmatrix} = \begin{bmatrix} T_s Y_\delta + 1 & T_s Y_\dot{\psi} \\ T_s N_v & N_{s+1} \end{bmatrix} \begin{pmatrix} v_k \\ \dot{\psi}_k \end{pmatrix} + \begin{pmatrix} Y_\delta \\ N_\delta \end{pmatrix} \delta_v \quad (3.15)$$

- Input:
  - $u$ , longitudinal velocity
  - $\delta_v$ , steering wheel angle
- State of the system:
  - $v$ , lateral velocity
  - $\dot{\psi}$ , yaw rate
- Measurement:
  - $\delta_v$ , steering wheel angle
  - $\dot{\psi}$ , yaw rate
  - $u$ , longitudinal velocity

Moreover, from the state computed, the yaw rate estimation by the model is compared with the measured one and then the state of the system is corrected as explained previously on the Kalman filter procedure.

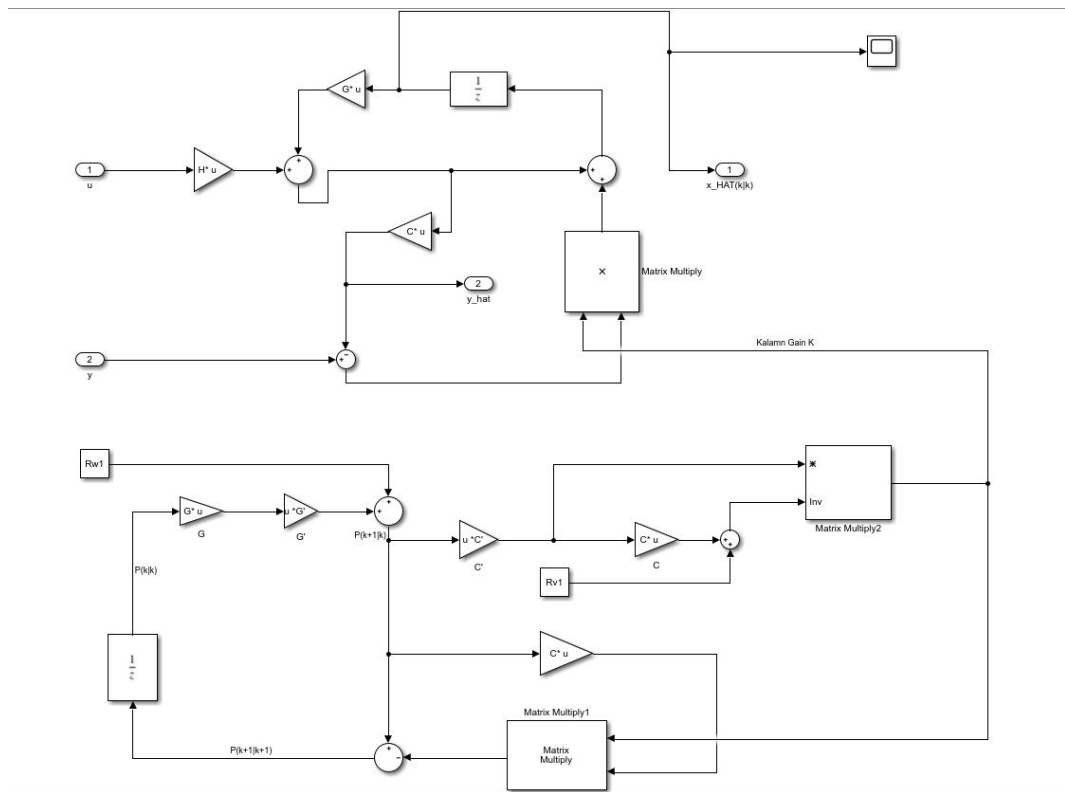


Figure 3.4: Kalman filter in Simulink

## Chapter 4

# Testing and instrumentation procedure

### 4.1 Balocco proving ground

Balocco Proving Ground (Fig.4.1) is a group of automobiles roads in Balocco (VC), owned by FCA (Fiat Chrysler Automobiles S.p.a.). It is the main proving ground of FCA Italy.

Test track was built in the early 1960s for testing new cars, prototypes and racing cars. In the track is also hosted club and racing organization events. The overall area exceeds 5,000,000 square metres and it has over 65 kilometres of different types of test tracks.

The original design included a main circuit (the current Misto Alfa Romeo), within also another track of shorter duration, in addition to areas with special flooring and the reproduction of one country road.

When the Fiat Group purchased Alfa Romeo, the circuit came into the possession of the Turin house. Under the new management, the plant has been subjected to important changes, that have equipped it with several new tracks, with different characteristics and purposes. The following tracks (in addition to the aforementioned Misto Alfa and other secondary tracks), as in Fig.4.2:

- The high-speed track, is 7.8 km ring, with elevated curves characterized by a slope of up to 30%, which allows maximum speeds in excess of 300 km/h.
- The Langhe track, a reproduction of a secondary road (inspired precisely by the Langhe region), with numerous escape routes and variants that allow to derive different routes. It measures over 22 km, and is characterized by the irregularity of the road surface and the numerous ups and downs (slopes up to 14%), designed to undermine the attitude of the cars to be tested.



**Figure 4.1:** FCA Balocco Proving Ground

- Comfort track, with flooring designed for testing the suspensions.
- ABS track, used for brake testing.
- Off Road circuit.
- White track, designed to simulate conditions of low adherence to test the active safety systems installed on vehicles.
- NVH track, different surfaces to test road noise
- Durability track
- Dynamic platform, used for high lateral dynamic manoeuvres

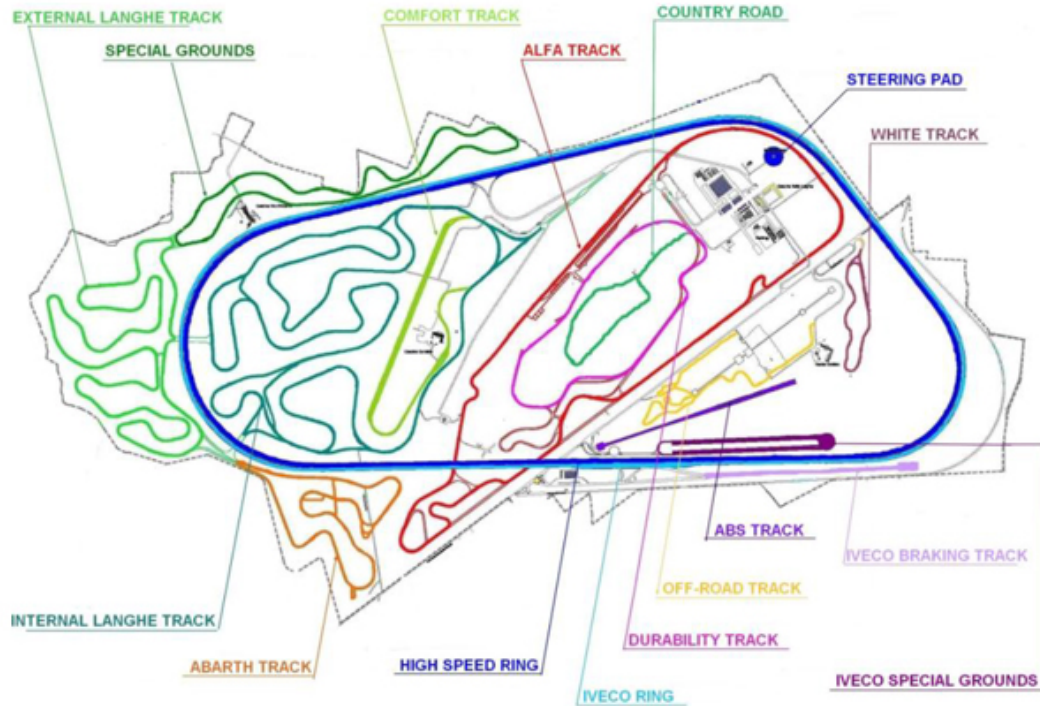


Figure 4.2: FCA Balocco Proving Ground layout

## 4.2 Maneuvers description

The application of ISO standards and robust legacy test procedures are good practices for the implementation of a reliable testing process. The “minimal” set of tests, which are defined by ISO standards, are covering the main aspects of vehicles behaviour on lateral, longitudinal and cross-coupled dynamics, as shown in the Fig.4.3.

Here a list of the main standard manoeuvre:

- Slow increasing steers: constant speed, steering wheel angle increases till the car limits;
- Steering pad: constant turn radius, speed increases till the car limits;
- SIN: constant speed and frequency, sinusoidal steering wheel angle input;
- RSI: constant speed, frequency sweep steering wheel angle input;
- SAC: constant speed while steering wheel angle increases, sinusoidal input;

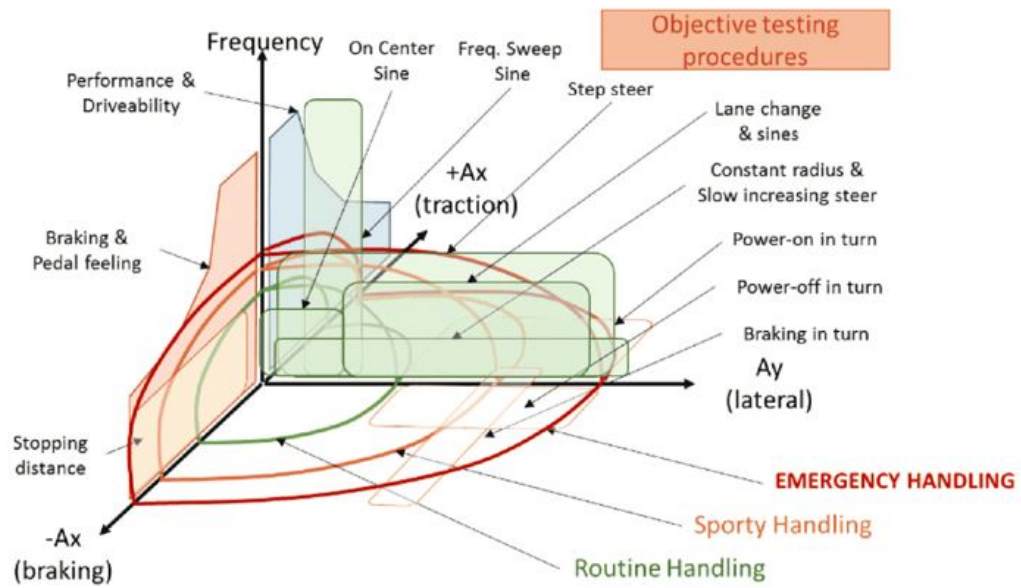


Figure 4.3: ISO standard manoeuvres

- Step Steer: constant speed, step input, steering wheel stays constant until the stationary condition is reached;
- CPS: step steer input is maintained for a few seconds;
- DLC: double lane change input (double CPS).

A brief description of the main manoeuvres by ISO normative are introduced, in the next pages.

### 4.2.1 Sinusoidal steering wheel cycles (ISO 7401)

The standard values for nominal speed are 60 km/h and 120 km/h.

**Test execution:**

At constant nominal speed (default 60km/h and 120km/h) and nominal gear (IV gear) it collects a steering wheel sinus with frequency 0.2Hz and a nominal amplitude, corresponding to a peak lateral acceleration ( $a_y$ ) of 0.2g and 0.4g.

**The sinus is made of three parts:**

- Initial offset part
- The sinus wave
- Final offset

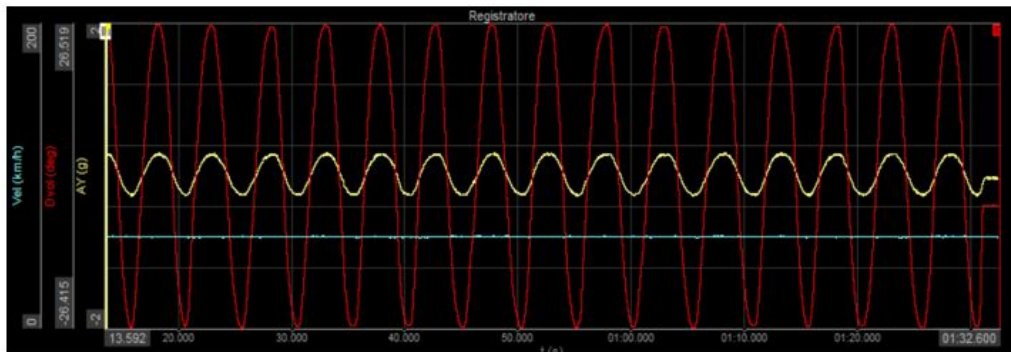


**Figure 4.4:** Sinusoidal steering wheel cycles with  $u = 60\text{km/h}$   $a_y = 0.25g$

**Threshold for acceptability:** Difference between nominal speed (usually 60km/h and 120km/h) and test medium speed (VEL)  $< 2.0\text{km/h}$

- $0.2g < \text{Peak lateral acceleration} < 0.25g$
- Steering angle sinus frequency  $0.2 \text{ Hz} \pm 0.1 \text{ Hz}$

### 4.2.2 Sweep steering wheel input (ISO7401)

This test shall be performed at least at three different amplitudes of steering wheel angle. The amplitude of the steering wheel angle may be a reference value for steering wheel angle or a value corresponding to a desired steady state lateral acceleration.

The standard value for nominal speed is 120 km/h, depending on the different market segments and so on for the lateral acceleration amplitude levels according to car classification, following this scheme:

- Speed = 120km/h - Lateral Acceleration = 0.3g – 0.5g – 0.7g

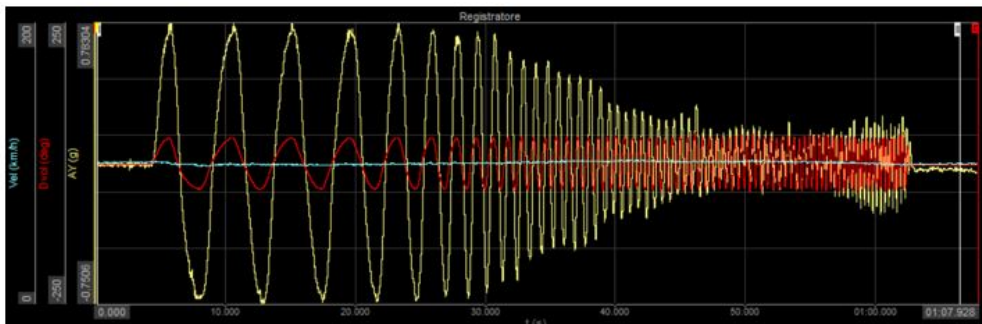


**Figure 4.5:** Sweep steering wheel input with  $u = 120$  km/h  $a_y = 0.7g$

**Test execution:** At constant nominal speed it collects a steering wheel sinus with increasing frequency from 0.2 Hz to 4 Hz and constant amplitude corresponding to the desired steady state lateral acceleration. The wave is made of three parts:

- Initial offset
- Increasing frequency sinus wave
- Final offset

### 4.2.3 Step steering input tests (ISO 7401) and steering wheel release

The standard value for nominal speed is 100km/h. According to the vehicle requirements and road friction coefficient, different speeds may be used, preferably in 20 km/h steps, as well as different steering wheel angles.

Test execution: The manoeuvre is made of four parts:

- Initial offset on straight line at constant nominal speed
- Step steer, then steering wheel angle constant
- Steering wheel release
- Final offset on straight at constant speed or with vehicle stopped

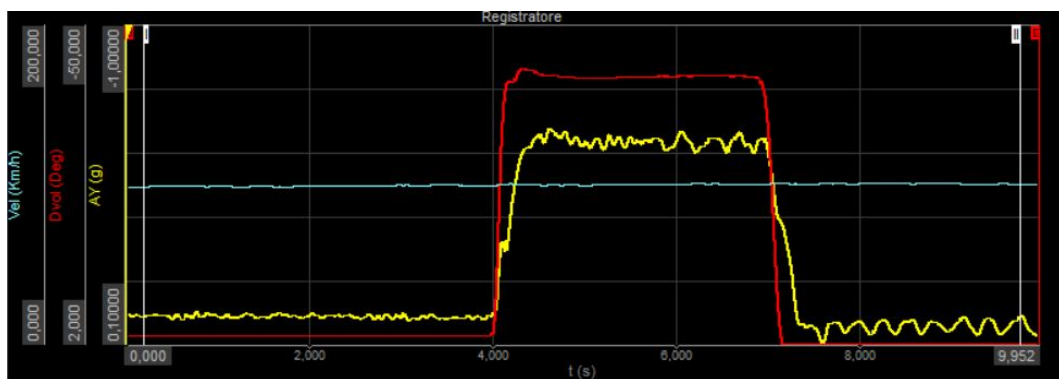


**Figure 4.6:** Slow increasing steer  $u=100\text{km/h}$

The test shall be performed in IV gear, at constant gas pedal position, if not differently specified. It might be made at different steering wheel angle. It must be paid attention to avoid overshoot of steering wheel angle after the step and keep steering wheel as constant as possible for at least 3 seconds, then release the steering wheel and let the vehicle self-align.

#### 4.2.4 Slow increasing steer

This comprehends also quasi-steady state behaviour in the linear range.

The standard value for initial speed is 100 km/h and the steering wheel angle shall increase with a rate of  $30^\circ/\text{s}$  up to  $180^\circ$ .

**Test execution** The test is made of four parts:

- Initial offset on straight at constant nominal speed
- Steering wheel angle ramp, increasing at a rate of  $30^\circ/\text{s}$ , up to  $180^\circ$  (duration = 6s)
- Hold final constant value (duration  $> 3$  s)
- Final offset on straight or vehicle stopped (duration  $> 2$  s)

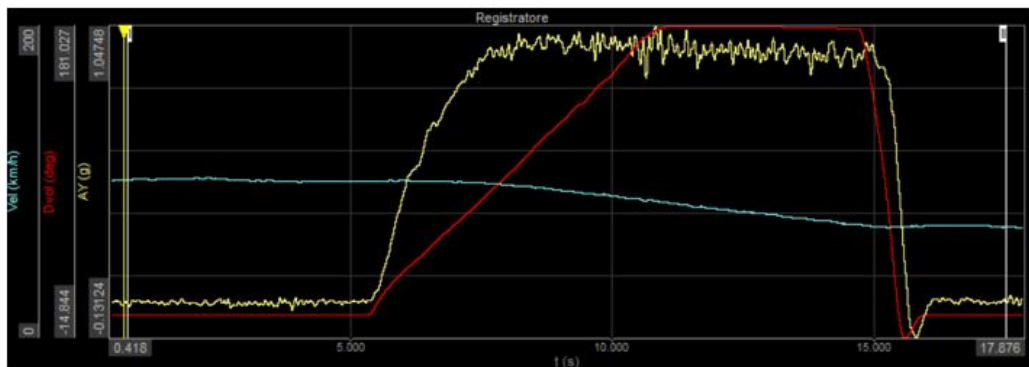


**Figure 4.7:** Slow increasing steer  $u=100\text{km/h}$

During the initial offset, the steering-wheel shall be subject to zero steer torque input. The recommended method to achieve this is to drive the vehicle under free steering control (hands free). In the whole test the gas pedal position shall remain fixed and the test is executed in IV gear if not different specified.

- Threshold for acceptability
- Difference between nominal speed (usually  $100\text{km/h}$ ) and test initial speed (VEL)  $< 2.0\text{km/h}$
- Steering angle speed (DVP) =  $30^\circ/\text{s}$

## 4.3 Instruments

### 4.3.1 IMU

An inertial measurement unit or inertial platform (also known as simply IMU) is an electronic system based on multiaxis combinations of precision gyroscopes, accelerometers and magnetometers, which allow monitoring the dynamics of a moving vehicle, which can be used by the computer or on-board control unit to implement any corrective measures.



**Figure 4.8:** Example of an imu (Kistler)

All components are combined in one housing and only one 4 wire cable leads to the connector. All sensor data are transferred to the data recorder via a bus line.

The inertial measurement unit measures up to six dimensions: yaw, roll and pitch rate as well as lateral, longitudinal and vertical accelerations. For the measurements the inertial measurement unit uses measuring elements in surface micromechanics. The yaw-rate sensor's measuring element works according to the Coriolis principle, meaning it utilizes the inertia force of an oscillating mass in a rotating system. Due to the high resonance frequency of 25 kHz and the closed drive and evaluation unit, the measuring element is very insensitive to mechanical interference. Acceleration is measured on the basis of the capacity change in the micromechanical structures.

The inertial measurement unit contributes to the functionality of active and passive safety systems and the airbag control unit as well as to vehicle test. The

inertial measurement unit is available for a multitude of automotive applications as well as for future advanced driver assistance systems functions and automated driving.

### 4.3.2 Optical sensor

Using a high-intensity light source to illuminate the measurement surface, the optical component of the Kistler sensor observes the stochastic microstructure of the surface via an objective lens.

The only way to obtain a good and reliable measure of sideslip angle is to use a 2-axis optical sensor (such as Kistler) on the car, usually on the front or on the back. The instrument shines a light on the asphalt and determines the two-speed components ( $u$  and  $v$ ) obtaining so the sideslip angle.

As explained before, this instrument cannot be used on the series production vehicles and it is usually forbidden also for racing cars. For these reasons, it is necessary to find a reliable method to estimate the sideslip angle.



**Figure 4.9:** Example of an optical sensor (Kistler) used for vehicle dynamics testing

The acquired optical signal is projected onto a periodic prismatic grating within the system, where it is multiplied as details of the surface microstructure move across the grating.

Resultant spatial frequencies are integrated over the sensor field to generate a correlated average value. The electronic signal-processing component of the system utilizes tracking filters to determine the representative centre frequency, which is derived by calculating a mean value based on the variance in the frequency spectrum. This representative centre frequency allows reliable counting of signal periods, which are directly proportional to the distance that the observed surface has travelled relative to the sensor. Using this information, speed data can be derived for a gated length measurement.

### 4.3.3 Universal measurement steering wheels

Steering wheels sensors are designed for automotive testing. This generation of transducers incorporates numerous technological functions, such as:

- Angle reset, torque calibration
- A Start trigger signal to the remote data acquisition system.
- Optical coder processing to prevent the need for external TTL electronics
- Five simultaneous analogue output signals
- Suppression of the bearing friction influence on torque, allowing high accuracy for low torque measurements
- Low profile design retains the same driving conditions as with standard steering wheels
- The sensor assembly can be operated:
  - The sensor can be screwed on shaft
  - Easily mounted on any road vehicle by optional flanges
- Optional steering stops adjustable between  $\pm 15^\circ$  to  $\pm 165^\circ$  are available. These stops fold automatically for safety.



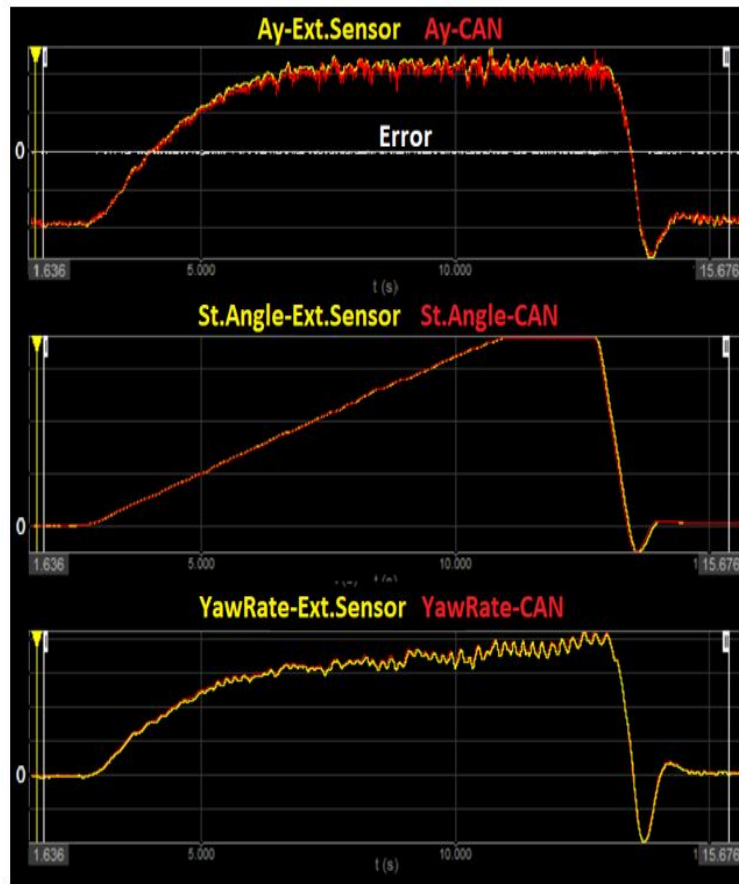


**Figure 4.11:** Comparison between  $a_y$ , Steering angle and Yaw Rate measured by CAN and by external sensors

#### 4.4.1 Typical operations performed on the signals

The signals obtained by the acquisition are not ready to be used, some post-processing steps must be done; FCA exploits a self-made software for the signal analysis, which is able to make some basic operations. This software is good at compensating some physical limits of the measures, in particular:

- Sensors position
- Signal shifting

Indeed, sensors are not positioned in the car centre of gravity; this means that the measured values can be affected by kinematic and geometrical inaccuracy.

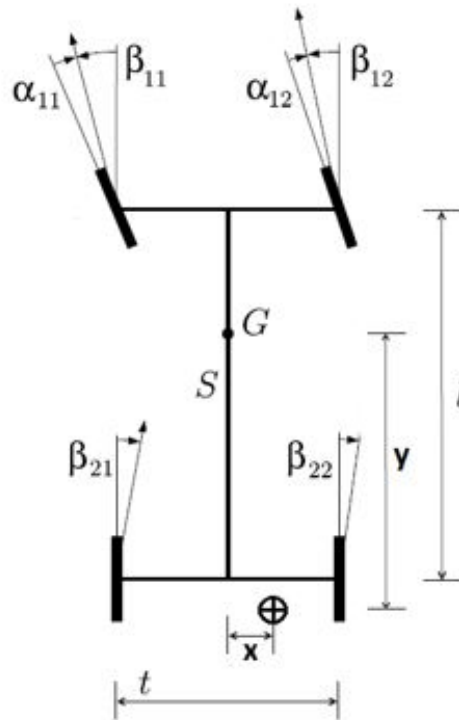


**Figure 4.12:** showing tyres VSA angle and the typical optical sensor position for tests

The software uses the sensors coordinates to compensate the geometrical errors. Then, for example, it employs other measured signals like the angular unsprung mass position to rectify the lateral acceleration. Although the correction is not so relevant for the other signals, it is for the sideslip angle. The geometrical correction is more important than the kinematic, indeed the last one can be neglected. The procedure is analogue to the one used to pass from the tyre VSA to the centre of gravity one.

About the signal shifting, the measures can be subject to a drift from the beginning to the end of the manoeuvre; for example, even though the steering wheel is equal to 0 at the beginning and at the end of the manoeuvre, VSA could start from 0 and finish with a different value. This phenomenon is compensated by a linear correction, which puts the VSA (such as other signals) to zero. Another operation to do is the measures offsetting: it is necessary because, although the accuracy of the sensor is not influenced by the mounting process, the absolute measured values are. For this reason, all the manoeuvres start from a neutral zero-condition:

$$\begin{cases} a_x = a_y = \dot{\psi} = \delta = 0 \\ u = \text{constant} \end{cases}$$

So that it's easy to identify a  $\Delta t$  for the offset operation. It's important to convert the physical quantities to the right unities of measurement. This is not a problem for the Artificial Neural Network because the determination of the links between different parameters is independent on multiplier factors. On the contrary, Kalman filter based estimator employs a specific single-track model which needs the right units. The steering wheel angle must be transposed to the wheel angles so that it must be divided for the medium steering rate. After this post-process, the measures might be used, but in the case of significant noise, an additional work is useful and recommended. There are some unpredictable factors which can change the noise intensity; Furthermore, sometimes some filters are applied to clean up the signals:

- Low-pass filter
- Moving-mean filter

The interesting frequencies for the longitudinal and the lateral dynamics are the lower ones; it's really hard to exceed the 4 Hz in these conditions and, however, over 2÷2.5 Hz the behaviour is negligible for the characterization of the vehicle dynamic. In the first acquisition phase the signals are already filtered over 10 Hz, by the software used; due to the noise, if it was useful the operation was repeated till 5 Hz or lower in case of necessity. Obviously, this operation must need a final check to verify the coherence of the values: loss of signal information must be avoided. In case of strong noise which produces rapid fluctuations around the right value, a moving-mean filter was applied, limiting this problem.

#### 4.4.2 Command *lsqcurvefit*

This command determines the unknown parameters by finding the curve that minimizes the sum of the squares of the distances between the observed data and those of the curve that represents the function itself. In order to operate it requires:

- A fit function in which there are unknown parameters to be determined
- Data to perform the fit
- An initial value  $X_0$  containing the values of the first attempt parameters from which to start the iteration

The function to be minimized (respect to  $X$ ) is the following:

$$F(X, k, r) = \sum_{i=1}^n (y(X, k_i) - r_i)^2 \quad (4.1)$$

Where:

- $y$  is the function chosen for the fit
- $k_i$  is the independent variable
- $n$  is the number of samples
- $r_i$  is the value to be fit
- $X$  is the vector containing the values of the coefficients to be determined.

# Chapter 5

## Handling experimental analysis

### 5.1 Introduction

In this chapter, an handling performance comparison will be shown and explained. An handling comparison might be done between type of cars, tyres or rims.

The goal of this chapter is to analyse a standard handling tyres comparison then in chapter six to verify if the tyres performance gap is respected by the predictive model. In chapter six, the sideslip angle will be the focus, although in this chapter wider analysis will be made.

The analysis starts with the vehicle preparation, all the sensors prepared in the car in a specific position of the analysis, below the sensors list and their position:

- IMU positioned next to the gear box
- Optical sensor mostly on the back of the car
- Universal measurement steering wheels

Once the vehicle is prepared, basic measures of the car, such as weight and wheel base, are made. Furthermore, also suspension, steering wheel and engine are verified as shown in Fig.5.1.

The handling analysis might be split in two parts:

- Subjective
- Objective

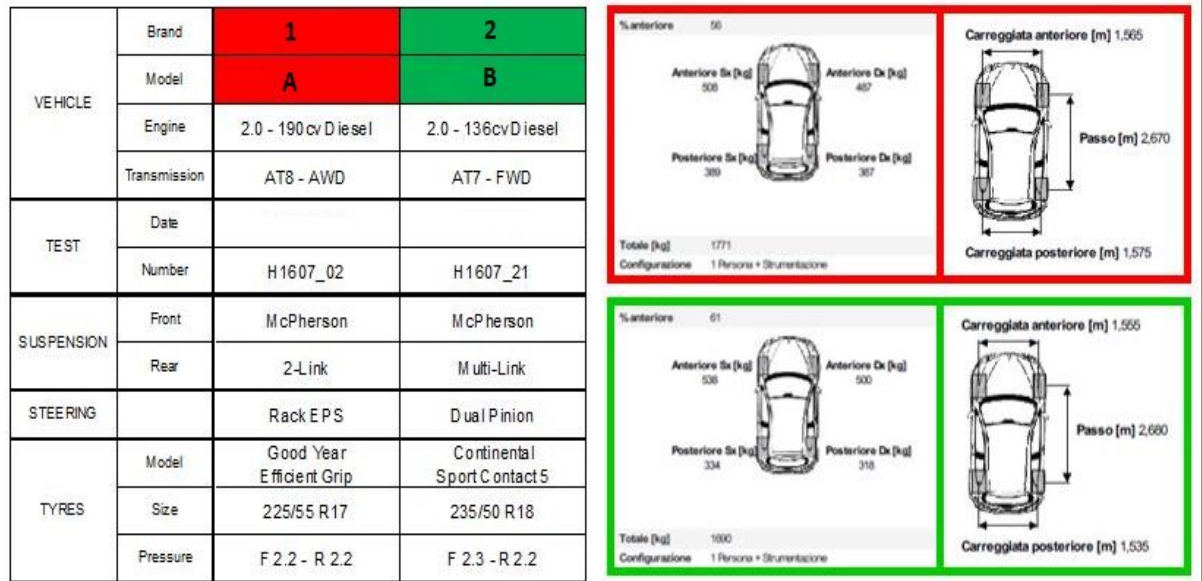


**Figure 5.1:** Example of vehicle data comparison

The subjective and objective analysis are made to be compared, indeed the objective data should respect the driver perception. In this thesis the subjective analysis will not be debated.

The next step is data acquisition; during the manoeuvres the driver is assisted collecting the data by the test engineer who also verifies that the manoeuvres are correct. Moreover, data are double checked by the laboratory and then can be used by the performance engineer. This chapter will focus especially in the last part.

The performance engineer analyses the signals and reports the results, making a conclusion about the comparison performance.

## 5.2 Tyres comparison

In tyre testing phase, several types of tyres are tested on the car, different brand, rim dimension and environmental conditions, for usually more than two loops.

In terms of handling analysis, a lateral dynamic steady state behaviour and a lateral dynamic transient behaviour analysis are made, either considering the routine handling (up to 0.4g lateral acceleration) and the sport handling (higher lateral acceleration). This distinction is important due to the fact that a car depending on its market positioning can be targeted toward a more or less sporty attitude, especially in terms of under and over steering. Indeed, understeering is

always preferred in standard cars for safety reasons, being more predictable than oversteering.

In this section, an hybrid car, segment C is considered with three different types of tyre.

Brand	Dimension
Supplier 1	225/55 R18
Supplier 2	225/55 R18
Supplier 3	235/55 R18

### 5.2.1 Steady state behaviour analysis

In this part the data extrapolated from the ramp steer manoeuvre, that is the steady state reference manoeuvre, will be shown. This manoeuvre is made at 100 km/h as explained in chapter four. Moreover this manoeuvre is reported, by the FCA software, at constant trajectory radius (40 m).

In steady state three curves are the most significant:

- Understeering curve
- Sideslip angle curve
- Axles cornering stiffness

As shown in Fig.5.2 the understeering curve and in Fig.5.3 the gradient understeering curve.

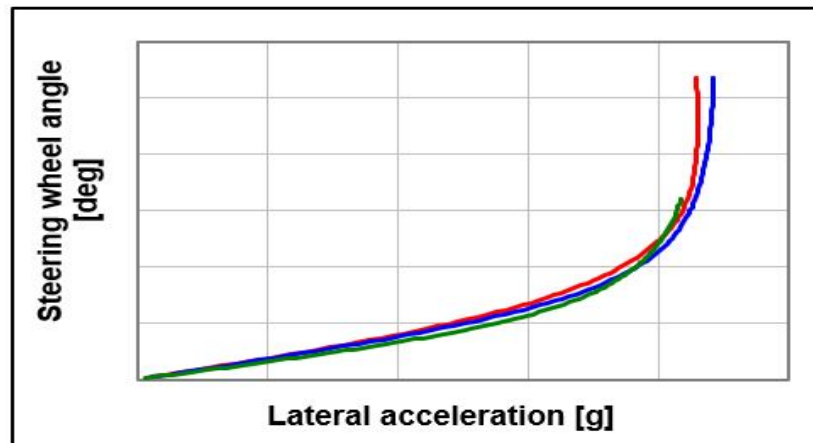
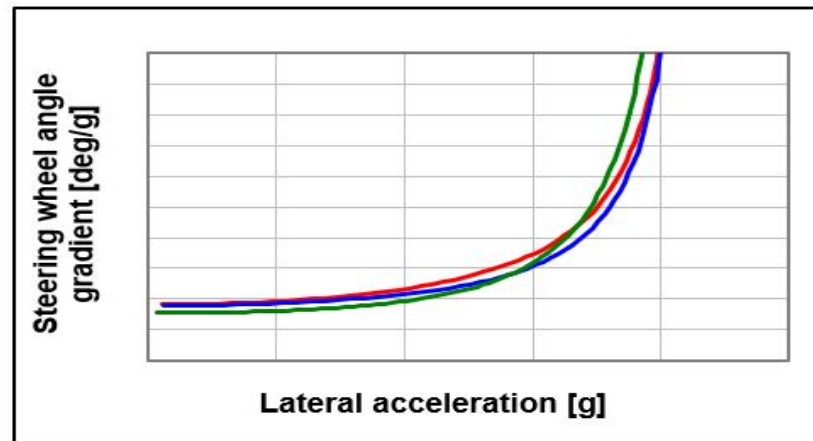


Figure 5.2: Understeering curve



**Figure 5.3:** Gradient understeering curve

Although there are not wide differences, supplier 3 has a lower understeering than the other two tyres, tested in the usual customer use range.

Moving towards the limit, the tendency is the opposite: supplier 3 reaches lower values of lateral acceleration and it has the highest gradient steering wheel angle (16% respect to the supplier 2 at 0.7g). In terms of lateral acceleration the supplier 2 reaches the maximum with a 3% of gap respect to supplier 3.

The Sideslip angle curves are reported at constant maneuver radius (40 m). As shown in Fig.5.4 the sideslip angle curve and in Fig.5.5 the gradient sideslip angle curve.

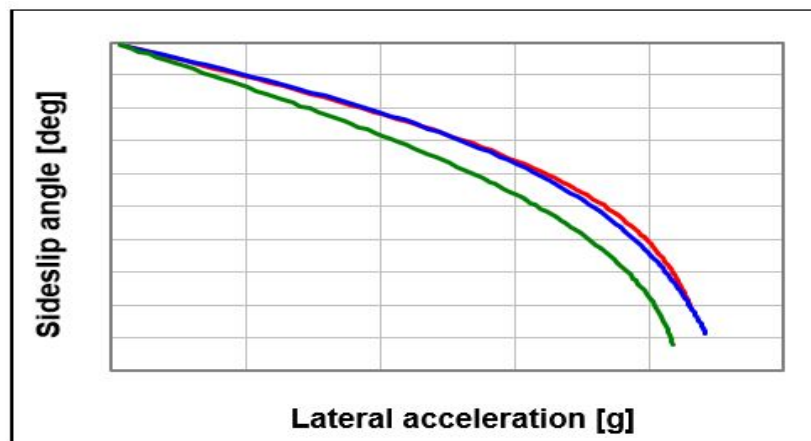


**Figure 5.4:** Sideslip angle

As widely explained in the previous chapters, the sideslip angle exhibits the vehicle stability. Indeed it is an important parameter to analyse, especially in steady state behaviour. As shown in Fig.5.4 the supplier 3 has the highest sideslip angle, either in linear and in tyres saturation behaviour. At 0.4g lateral acceleration, the supplier 3 gradient sideslip angle is 22% higher than the supplier 1. The number 1 and 2 are similar in linearity, however the supplier 1 is slightly better between 0.6g and 0.85g.

Reaching the limit handling, supplier 3 has a faster growth of sideslip angle assuming a less stable behaviour.

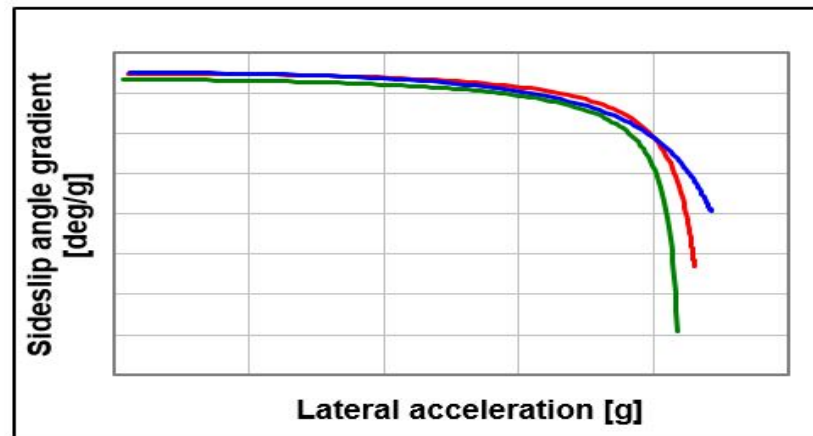


**Figure 5.5:** Gradient sideslip angle

In Fig.5.6 front and in Fig.5.7 rear cornering stiffness curve is shown.

The cornering stiffness, is a parameter that takes into account the whole vehicle stiffness, however it strongly depends on the tyres. Furthermore cornering stiffness analysis might help understanding the tyres behaviour. Moreover the sideslip angle is strongly depending on the front and rear cornering stiffness and in chapter six the sideslip angle estimation method will be shown as well as the cornering estimation.

Supplier 3 has a lower front and rear cornering stiffness at every lateral acceleration. At low acceleration, the supplier 3 rear is less stiff, moreover also a big gap between front and rear is present. This might explain the supplier 3 sideslip angle curve, previously shown. Indeed, with supplier 3 having the front and rear cornering axles more flexible, makes the vehicle more unstable. The supplier 1 and 2 do not differ substantially, neither in the front nor in the rear.

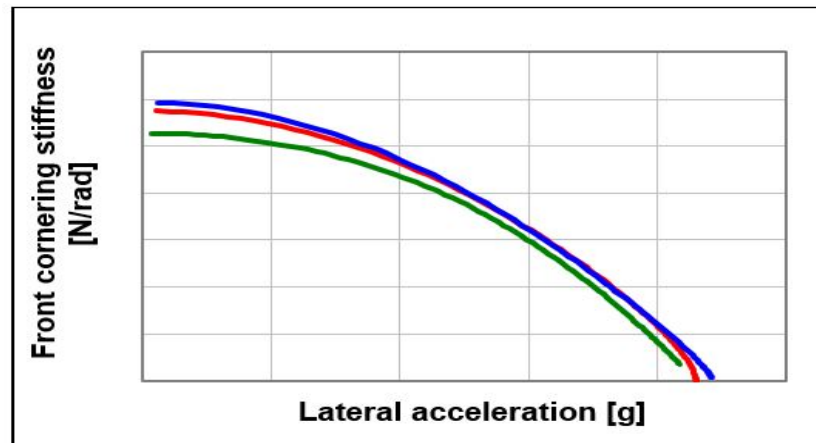


Figure 5.6: Front cornering stiffness

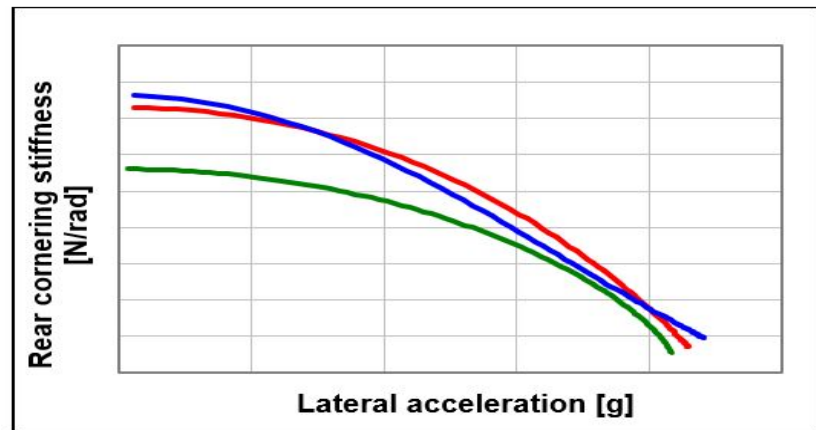


Figure 5.7: Rear cornering stiffness

### 5.2.2 Transient behaviour analysis

Since the interest is analysing input-output relationship for the observer-based model, measurable quantities of the system which strongly influence the vehicle sideslip angle are analysed, such as lateral acceleration, yaw rate and steering wheel angle.

In this part the data extrapolated from the sweep frequency manoeuvre, that is the transient reference manoeuvre, will be shown. This manoeuvre is made with 120 km/h nominal speed as explained in chapter four.

This analysis is made through the Bode plot, that consists of two graphs

representing the amplitude and phase of the complex frequency response function respectively. In this chapter, the delay is considered instead of the phase to maintain the company standards. However, the phase/delay plots are very significant for the thesis goal due to the fact that the variation in phase shift between the measurements and sideslip angle makes the estimation more difficult.

The frequencies analysed are usually  $0 \div 4$  Hz, due to these frequencies includes all the vehicle dynamic fields that a car can reach.

Furthermore, the transient analysis might be made at different lateral acceleration, usually 0.3g, 0.5g and 0.7g to have a wide vision of the vehicle behaviour in all the conditions.

In this case, four transfer functions are considered at two different lateral acceleration (0.3g and 0.5g):

- Yaw rate/Steering wheel angle
- Lateral acceleration/Steering wheel angle
- Yaw rate/Lateral acceleration
- Sideslip angle/Steering wheel angle

Firstly, the sweep frequency manoeuvre at 120km/h nominal speed at 0.3g lateral acceleration

In Fig.5.8 gain and delays of the yaw rate/steering wheel angle are shown.

The yaw rate Bode plot exhibits a typical second order system behaviour. The peak value is at a frequency that is due to the fact that as the frequency increases, there is less time for a rotational speed to grow for a given acceleration. Moreover, an important parameter is the phase shift for the transfer function between yaw rate and steering wheel angle, because it determines reactivity of the front axle. Given an increase of steering wheel angle, the front slip angle increases, therefore, yawing torque given by the front tyres will increase. A minor factor can also be found in the transient behaviour of the tyre due to its elasticity. The classic parameter used to represent the tyre transient behaviour is the relaxation length.[15] As the frequency grows, the force produced by the tyre tends to be lower respect to the steady-state value.

At 1 Hz as well as in static condition, the yaw rate gain is similar for the three tyres, the gap is less than 2%. The number 1 has a maximum gain higher than the others, 4% of gap, moreover the supplier 1 has higher yaw natural frequency (15%). At higher frequencies, the response filtering between steering wheel angle and yaw rate does not change with the three tyres.

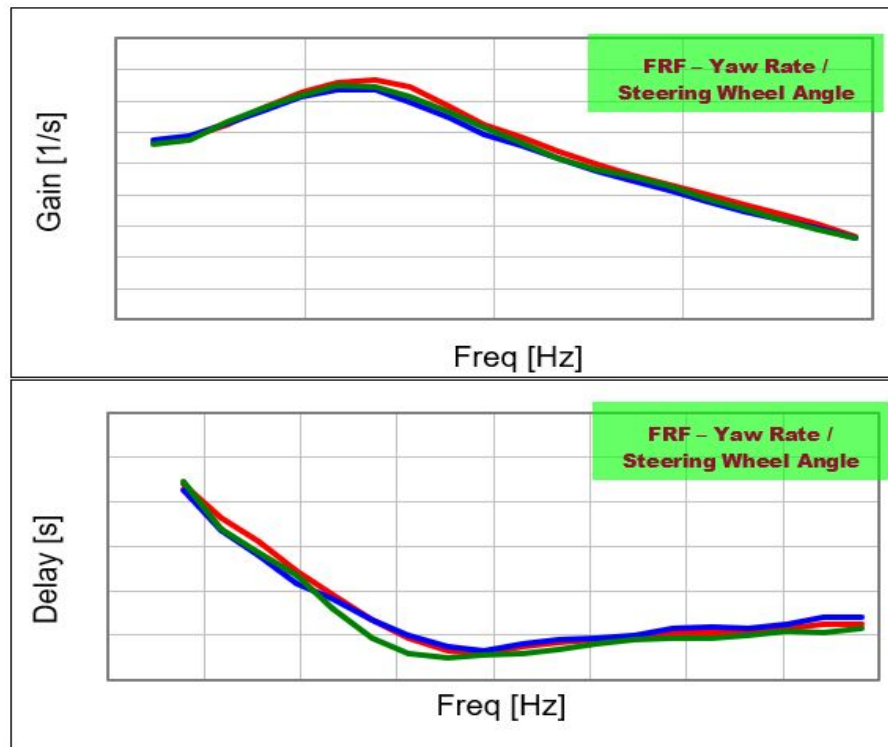


**Figure 5.8:** Bode plot between Yaw rate and steering wheel angle in a sweep frequency manoeuvre at 0.3g lateral acceleration

In terms of delays, the supplier 3 has higher values in all the frequencies considered. The number 1 and 2 are practically the same, although the supplier 1 has a faster response at low frequencies.

In general, in the front axle, there are not a big differences through the tyres.

In Fig.5.9 gain and delays of the lateral acceleration/steering wheel angle are shown.

The gain diagram looks like a low-pass filter as well. The cutoff frequency depends mainly on mass and inertial properties of the vehicle. Indeed, the natural frequencies are practically the same.

As explained above, when yaw rate increases, front slip angle grows while the rear slip angle decreases. This reduction makes the total lateral force generated by the tyres lower, despite the growth in front slip angle.

The reason is that the slip angle generated by the front tyre mainly depends on steering angle, and only a small part of the generated angle is due to the yaw rate, instead to the rear tyres where slip angle depends strictly on yaw rate and lateral

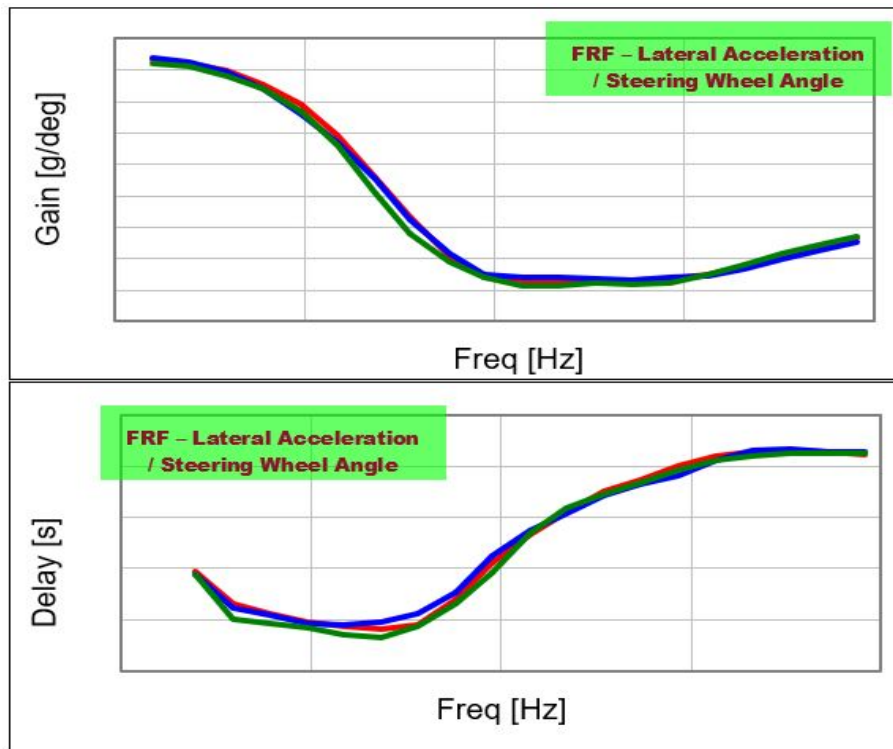


**Figure 5.9:** Bode plot between Lateral acceleration and steering wheel angle in a sweep frequency manoeuvre at 0.3g lateral acceleration

velocity.

Also, for high frequencies front and rear slip angles are almost in counter phase. Indeed, lateral forces generated by the front and rear wheels are opposite so a reduction in rear slip angle makes the total lateral force grow.

Although there are not wide differences, in routine handling, the supplier 1 has an higher lateral acceleration gain (at 1 Hz 4.5% of gap) due to the combination between high value of cornering stiffness and low understeering gradient. However for supplier 3, the vehicle response (delays) is higher than type 1 and 2, especially in the usual customer use range.

In Fig.5.10 gain and delays of the yaw rate/lateral acceleration are shown.

For the rear axle, at low frequencies, there are not big differences, however in terms of maximum gain the tyres behaves differently. Indeed the supplier 3 has the highest maximum yaw gain, followed by the number 1 with a wide gap respect to the supplier 2 (13%). The supplier 1 and 2 have exactly the same natural frequency, higher than the supplier 3 (3%). Moving towards to higher frequencies, the gap is

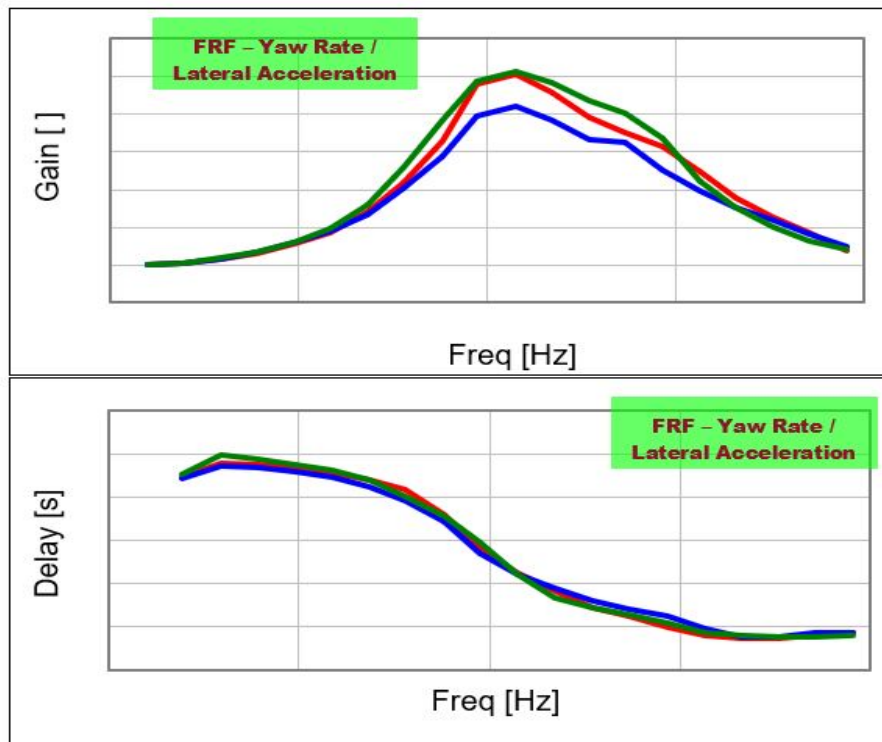


**Figure 5.10:** Bode plot between Yaw rate and lateral acceleration in a sweep frequency manoeuvre at 0.3g lateral acceleration

closing as it approaches to 4 Hz.

In general, for the rear axle, supplier 3 behaves better than the others in terms of gain although in terms of delays there are not evident differences.

In Fig.5.11 gain and delays of the Sideslip angle/Steering wheel angle are shown.

Due to the sideslip angle high dependence on lateral acceleration and yaw rate, results found are significant in the design of the model, especially for the delays. Another important fact is that changing the vehicle type of tyres, even between very similar tyres, makes the front and rear slip angles vary different and so changing the results substantially.

At 1 Hz, as reference frequency, the tyre 3 obtain the highest value with a gap of 8% respect to supplier 2 that has the lowest, confirming the steady state analysis previously shown for the sideslip angle (Fig.5.4). Furthermore, the number 3 shows also the maximum gain, as expected from the beta steady state curve.

In terms of natural frequency, a big difference is present as gain plot shows. Moreover, the gap between the supplier 1 and 2 is 18%. Moving towards to higher

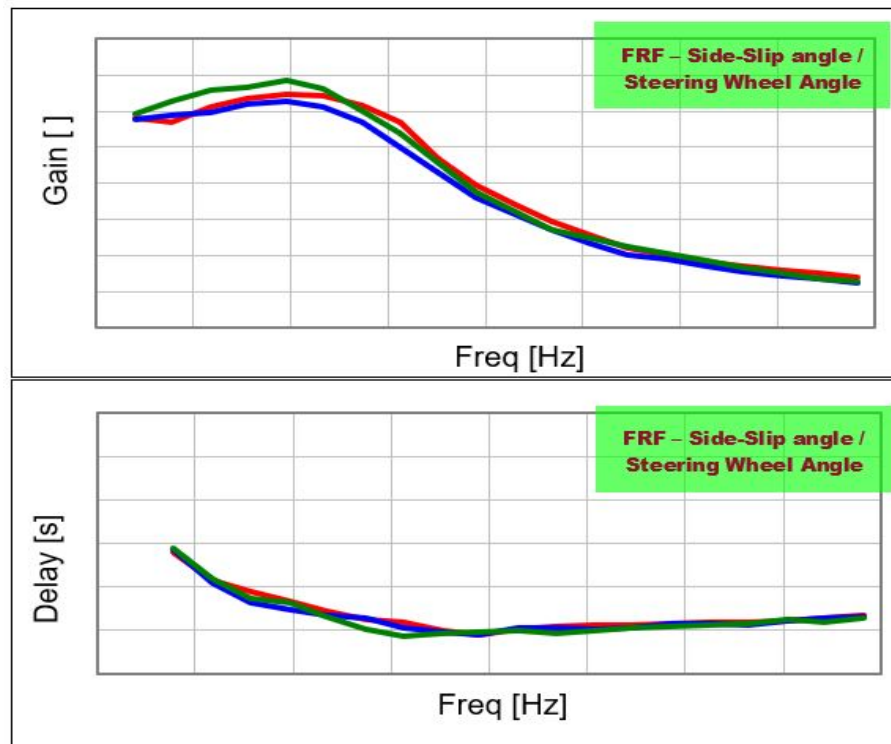


**Figure 5.11:** Bode plot between Sideslip angle and Steering wheel angle in a sweep frequency manoeuvre at 0.3g lateral acceleration

frequencies, the gain gap is closing as it approaches to 4 Hz.

In general, the steady state behaviour is followed, where the third supplier obtains the highest gain especially at low frequencies.

Secondly, the sweep frequency manoeuvre at 120km/h nominal speed at 0.5g lateral acceleration

In Fig.5.12 gain and delays of the yaw rate/steering wheel angle are shown.

At 1 Hz as well as in static condition, the yaw rate gain is similar for the three tyres, the gap is less than 2%, anyway the supplier 1 is the best. The supplier 1 has a maximum gain higher than the others, 3% of gap, moreover yaw natural frequency is practically the same for all three suppliers. In terms of delays, the supplier 3 has higher values at frequencies higher than 1 Hz. The number 1 is better than number 2 at low frequencies, at higher frequencies (higher than 1.5 Hz) the opposite situation is exhibited.

In general, for the front axle, there are not a big differences through the tyres, just a few differences in terms of delay.

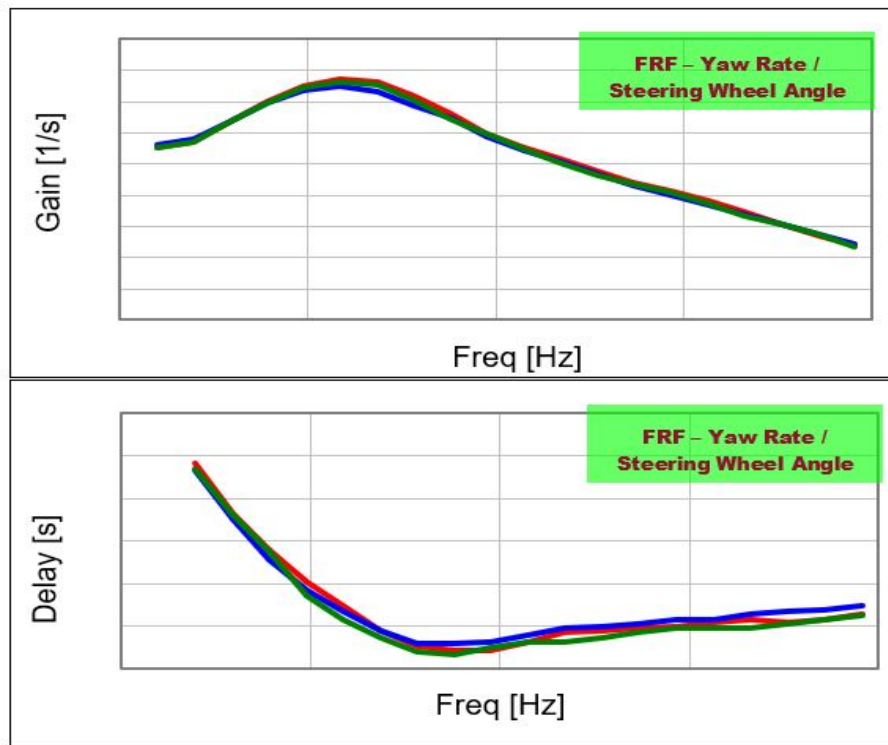


**Figure 5.12:** Bode plot between Yaw rate and steering wheel angle in a sweep frequency manoeuvre at 0.5g lateral acceleration

In Fig.5.13 gain and delays of the lateral acceleration/steering wheel angle are shown.

In linear range, routine handling, the supplier 1 has an higher lateral acceleration gain due to the lower understeering gradient. At 1Hz 4% of gap between supplier 1 and 3. Furthermore for supplier 3, the vehicle response (delays) is higher especially in routine handling.

In Fig.5.14 gain and delays of the yaw rate/lateral acceleration are shown.

For the rear axle, at low frequencies (up to 1.5 Hz), there are not differences however in terms of maximum gain the tyres behaves differently. Indeed the supplier 3 has the highest maximum yaw gain, immediately followed by the supplier 1, although a wide gap respect to the number 2 (13%) is exhibited. The number 2 has the highest natural frequency, higher than the supplier 1 of 7% and number 3 of 10%. At higher frequencies the gap is closing as it approaches to 4 Hz. In terms of delays there are not evident differences.

In general, for the rear axle, supplier 3 behaves better than the others in terms

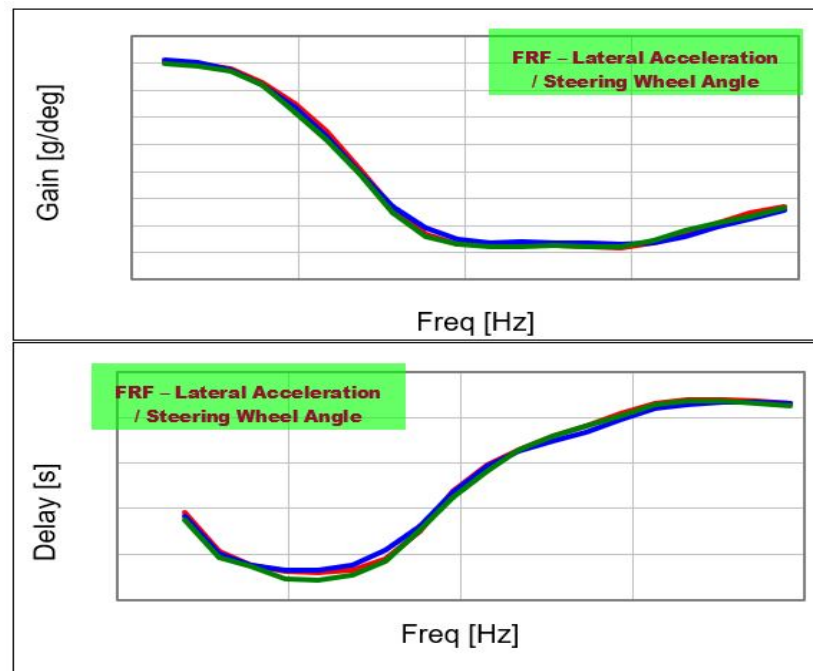


**Figure 5.13:** Bode plot between Lateral acceleration and steering wheel angle in a sweep frequencies manoeuvre at 0.5g lateral acceleration

of gain, although in terms of delays there are not evident differences.

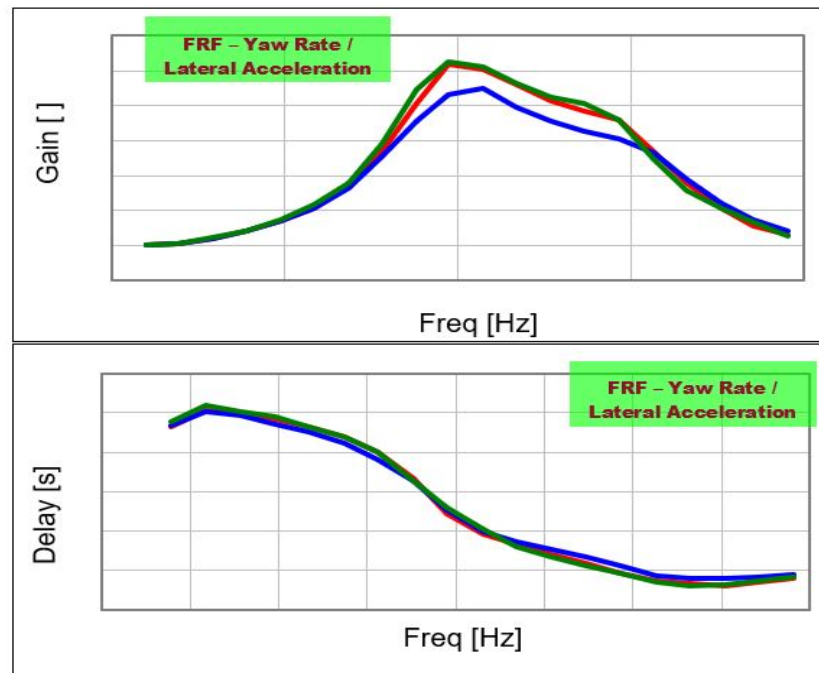


**Figure 5.14:** Bode plot between Yaw rate and lateral acceleration in a sweep frequency manoeuvre at 0.5g lateral acceleration

In Fig.5.15 gain and delays of the Sideslip angle/Steering wheel angle are shown.

At 1 Hz, as reference frequency, the tyre 3 obtain the highest value, as at 0.3g, with a gap of 6% respect to supplier 2 that has the lowest, confirming steady state analysis previously shown for the sideslip angle (Fig.5.4) and the transient analysis (Fig.5.11). Furthermore, the number 3 shows also the maximum gain, as expected from the beta steady state curve. In general the scenery is similar to the previous one at 0.3g lateral acceleration although the difference between the tyres performance is lower.

In terms of natural frequency, a big difference is present as gain plot shows. Moreover, the gap between the supplier 1 and 2 is 17%. Moving towards to higher frequencies, the gain gap is closing as it approaches to 4 Hz.

In these conditions, the transient behaviour (at 0.3g) and the steady state analysis is followed, where the third supplier obtains the highest gain especially at low frequencies.

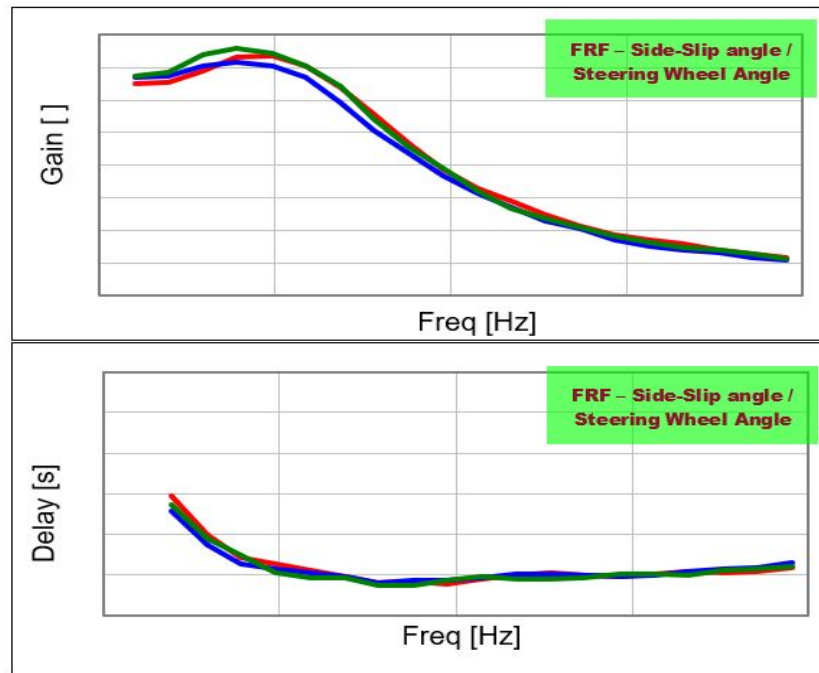


**Figure 5.15:** Bode plot between Sideslip angle and Steering wheel angle in a sweep frequency manoeuvre at 0.5g lateral acceleration

### 5.2.3 Conclusion

This comparison enlightens some characterizing issues making different handling behaviour of the 3 tyres:

- In STEADY STATE BEHAVIOUR tyre 3 has a bit lower understeering gradient, respect to the other in the usual customer range, and a faster growth of steering wheel angle towards the limit. However, it has also a much higher sideslip gradient with a less progressive growth near limit handling of sideslip angle, that means less stability and less maximum lateral acceleration.
- In TRANSIENT BEHAVIOUR the yaw natural frequency is the same for the all three suppliers, same lateral acceleration pass band, although supplier 3 has higher lateral acceleration comparing with a given yaw rate at 2 Hz. Sideslip angle greater for tyre 3 as in steady state, up to 2 Hz. In normal customer handling the three tyres behave similar.

# Chapter 6

## Sideslip angle estimation

### 6.1 Introduction

As widely explained, the goal of this thesis was to estimate the sideslip angle. Once the data were filtered, they were ready to be used to estimate the sideslip angle.

The bicycle model were picked because it is a good compromise between its complexity and its adaptability in this specific field. Moreover the idea behind this model is that sometimes it is not necessary or desirable to include the longitudinal vehicle dynamic, because it does not affect deeply the lateral stability of the vehicle.

Having the equations explained in chapter two that can be rearranged in:

$$\begin{cases} mu\dot{\beta} = Y_{\beta}\beta + (Y_{\rho} - mu^2)\rho + Y_{\delta}\delta \\ J_z u\dot{\rho} = N_{\beta}\beta + N_{\rho}\rho + N_{\delta}\delta \end{cases}$$

Where:  $\rho$  is the ratio between  $\dot{\psi}$  and  $u$ .

Stability derivative	Formulation	Definition
Damping-in-sideslip	$Y_{\beta} = C_f + C_r$	$Y_{\beta} = \frac{\partial Y}{\partial \beta}$
Lateral force/yaw coupling	$Y_{\dot{\psi}} = \frac{1}{u}(a_1 C_1 - a_2 C_2)$	$Y_{\dot{\psi}} = \frac{\partial Y}{\partial \dot{\psi}}$
Control force	$Y_{\delta} = -C_1$	$Y_{\delta} = \frac{\partial Y}{\partial \delta}$
Direction stability	$N_{\beta} = a_1 C_1 + a_2 C_2$	$N_{\beta} = \frac{\partial N}{\partial \beta}$
Yaw damping	$N_{\dot{\psi}} = \frac{1}{u}(a_1^2 C_1 - a_2^2 C_2)$	$N_{\dot{\psi}} = \frac{\partial N}{\partial \dot{\psi}}$
Control moment	$N_{\delta} = -a_1 C_1$	$N_{\delta} = \frac{\partial N}{\partial \delta}$

This is the model that in matrix version is used, with the aid of the Kalman filter, to estimate the sideslip angle.

The vehicle inputs necessary to set the car model are just a few:

- Mass
- Moment of inertia
- Wheelbase
- Mass distribution on the axles
- Front and rear cornering stiffness

Mass, mass distribution and wheelbase are easily measurable.

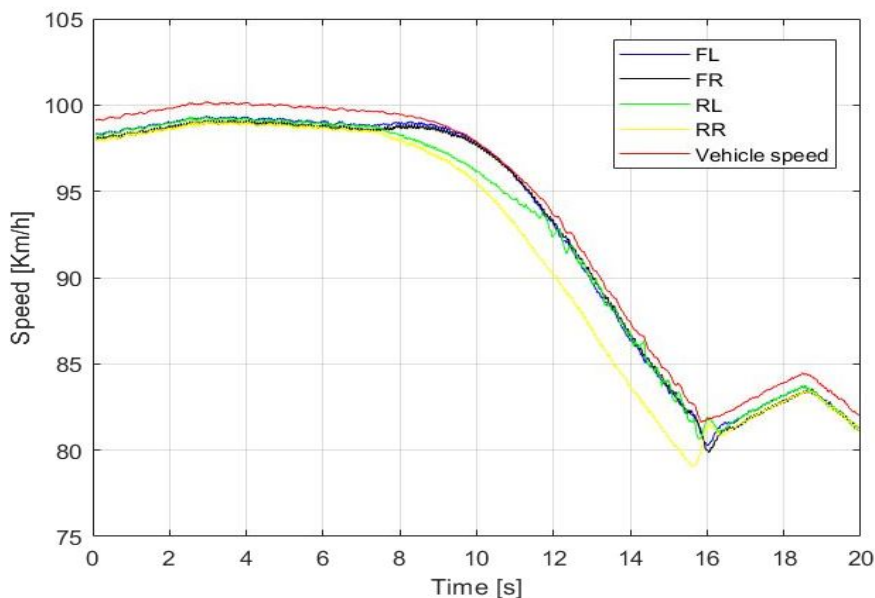


**Figure 6.1:** Wheels speed

Although the software developed in FCA can determinate the inertia by analysing a series of manoeuvres, the moment of inertia has been calculated with the geometric formula:

$$J_z = M_{front}a_1^2 + M_{rear}a_2^2 \quad (6.1)$$

Where  $M_{front}$  and  $M_{rear}$  are the masses respectively considered in the front and rear axle.

The FCA software can even compute the cornering stiffnesses. The software computes the cornering stiffnesses through a two degree of freedom bicycle model, having available the optical sensor measurements and so the sideslip angle. However the aim of this thesis was to estimate the sideslip angle without using the optical sensor.

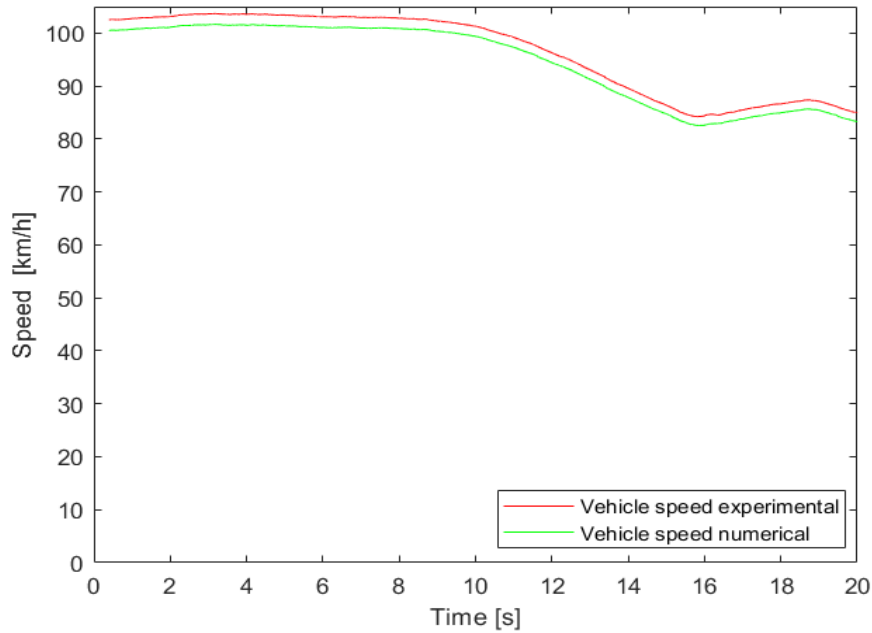


**Figure 6.2:** Vehicle speed estimation and measurement

Indeed as first approximation, the front and rear cornering stiffnesses were considered known, taking the two values from previous manoeuvres of the same car. Therefore, all the parameters were available.

The Fig.6.1 shows the four wheels speed and the vehicle speed estimation. Without having the optical sensor measurements, the vehicle speed might be computed through wheels speed measurements. The wheels speed measurements are available in all the standard cars and an estimation of the vehicle speed is made by the control unit. Furthermore, the Fig.6.2 shows a comparison between the vehicle speed estimation and the speed measured by the optical sensor.

## 6.2 Structure definition

The procedure was to estimate the sideslip angle with the standard bicycle model and the linear Kalman filter. The state-space (Fig.6.3) represents the model explained in chapter 3 and it is used in the all three methods in the same way. Below the system of equations is reposed:

$$\begin{pmatrix} v_{k+1} \\ \dot{\psi}_{k+1} \end{pmatrix} = \begin{bmatrix} T_s Y_\delta + 1 & T_s Y_\dot{\psi} \\ T_s N_v & N_{s+1} \end{bmatrix} \begin{pmatrix} v_k \\ \dot{\psi}_k \end{pmatrix} + \begin{pmatrix} Y_\delta \\ N_\delta \end{pmatrix} \delta_v \quad (6.2)$$

Where:

$$A = \begin{bmatrix} T_s Y_\delta + 1 & T_s Y_\dot{\psi} \\ T_s N_v & N_{s+1} \end{bmatrix}$$

$$B = \begin{bmatrix} Y_\delta \\ N_\delta \end{bmatrix}$$

$$C = \begin{bmatrix} 0 & 0 \\ 0 & 1 \end{bmatrix}$$

$$D = \begin{bmatrix} 0 \\ 0 \end{bmatrix}$$

The first method, considering the cornering stiffnesses constant along the manoeuvres as shown in Fig.6.3. The cornering stiffness estimation is made by the FCA software through the steady state standard manoeuvres. As in figure, the input were:

- $u$ : longitudinal speed
- $\dot{\psi}$ : Yaw rate
- $\delta_v$ : steering wheel angle
- $C_1$  and  $C_2$ : constant front and rear cornering stiffnesses

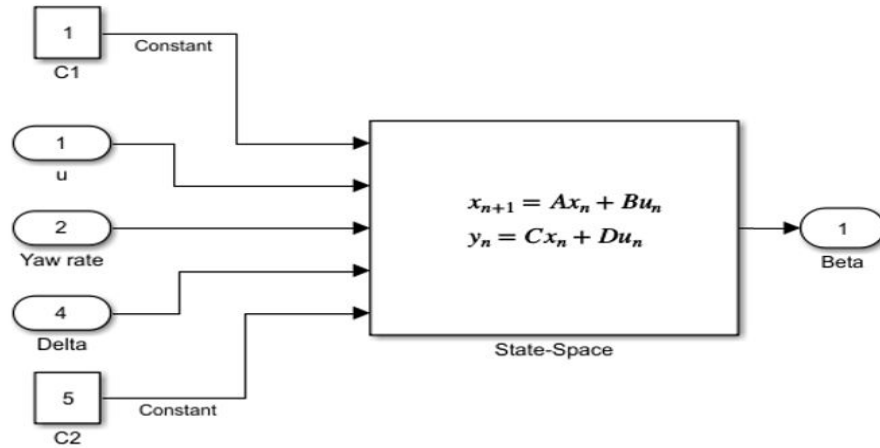


**Figure 6.3:** Simulink block Steady state reference manoeuvre with constant cornering stiffnesses

This method has been applied to ramp steer, showing especially at lateral acceleration higher than 0.4g that the numerical data do not follow the experimental one. This is probably due to the fact that the cornering stiffnesses values are kept constant along the manoeuvres.

The second method, three constant values of cornering stiffnesses were used, three for each axle as shown in Fig.6.4. The three values of cornering stiffnesses are picked on the basis of the lateral acceleration. Furthermore, the range was from 0g to 1.0g of lateral acceleration, divided in three steps 0.3g, 0.6g, 1.0g.

The maximum value of lateral acceleration has been decided, based on previous manoeuvres where this value has never been reached. Moreover, in standard cars this value is not repeatable, especially in routine handling. However, in sporty handling higher acceleration might be highlighted, such as 0.9g.

As in figure, the input were:

- $u$ : longitudinal speed
- $\dot{\psi}$ : Yaw rate
- $\delta_v$ : steering wheel angle
- $C_1$  and  $C_2$ : three constant values for front and rear cornering stiffnesses

This was done to obtain a method that could better adapt even at higher lateral acceleration. This method has been applied to the steady state manoeuvre to obtain a direct compare with the second method. The result shows a lower gap between the experimental and the numerical data, especially at high lateral acceleration.

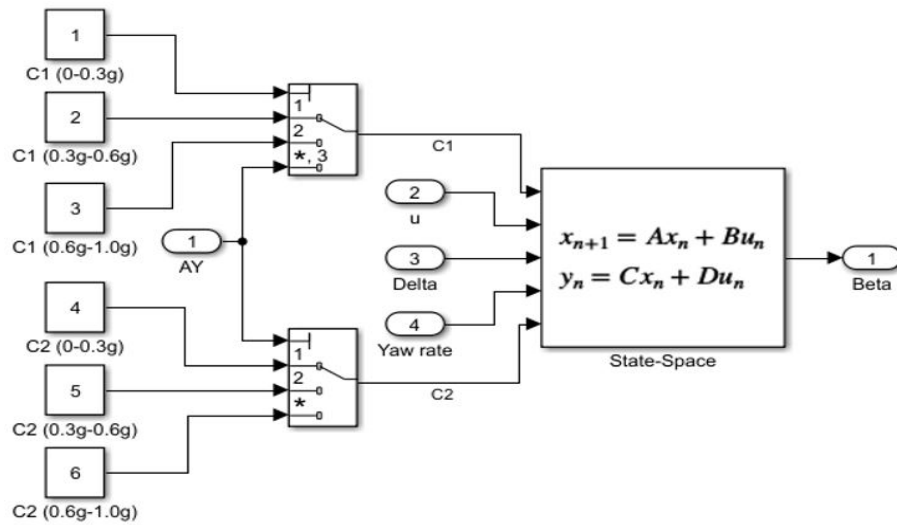


**Figure 6.4:** Simulink block Steady state reference manoeuvre with three values of cornering stiffnesses depending on the lateral acceleration

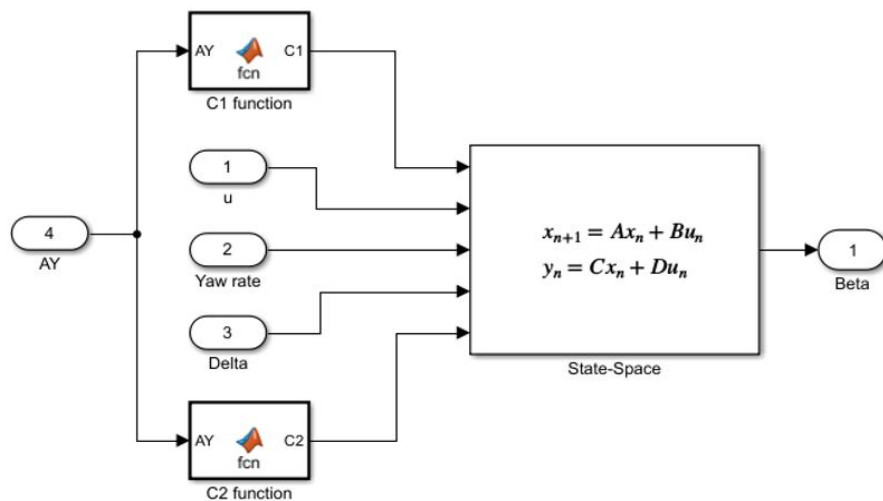


**Figure 6.5:** Simulink block Steady state reference manoeuvre with two functions of cornering stiffnesses

In the third method, the goal was to estimate the cornering stiffnesses, through the kinematic model, so that the cornering stiffnesses were computed every step through a parabolic function which depends on the lateral acceleration (Fig.6.5) and

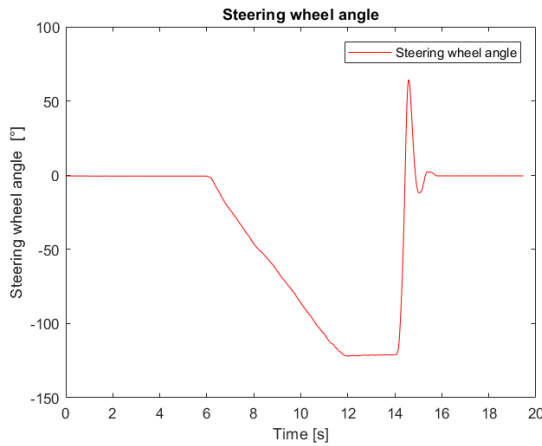
the data from FCA software were no longer needed. Once the cornering stiffnesses were computed, the method has been validated for the standard manoeuvres, for the sweep frequency and for LAP at constant speed. The method is further explained in paragraph 6.3.

The input were:

- $u$ : longitudinal speed
- $\dot{\psi}$ : Yaw rate
- $\delta_v$ : steering wheel angle
- $a_y$ : Lateral acceleration

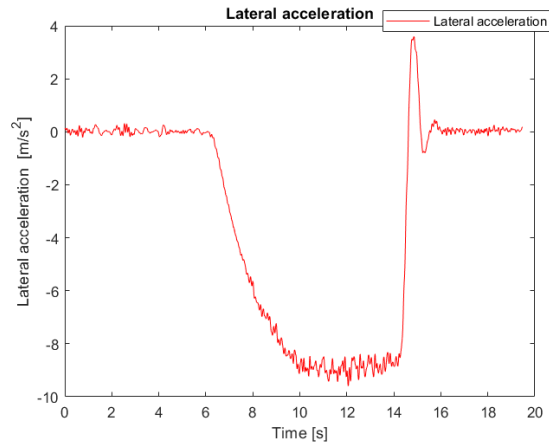
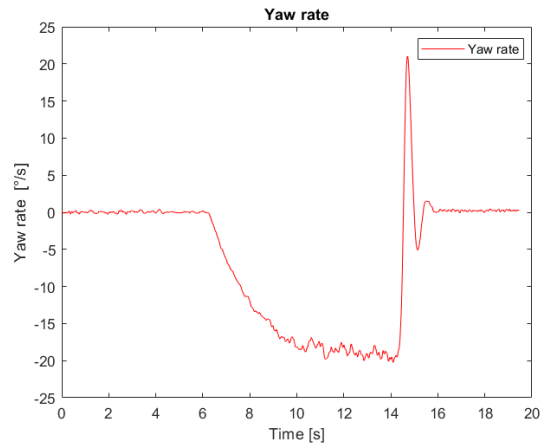
### 6.3 First method

The first method, as shown in the Simulink block (Fig.6.3), considers the cornering stiffnesses constant, one for the front and one for the rear. The state-space is the model showed in Eq. 6.2. This method has been applied at the steady state reference manoeuvre, that is the ramp steer at constant nominal speed with constant steer angle rate. In this specific case a 100 km/h nominal speed and a 20 °/s steer angle rate.



**Figure 6.6:** Steering angle

Furthermore, the cornering stiffnesses were given by the FCA software from previous manoeuvres, taking the value at lateral acceleration equal to zero ( $a_y = 0$ ). Moreover, the longitudinal speed was approximated with the vehicle speed.

**Figure 6.7:** Lateral acceleration**Figure 6.8:** Yaw rate

The first result obtained from the model shows that the gap between experimental and numerical sideslip angle is mainly in high lateral accelerations such as more than 0.45g. This issue is probably related to the fact that the cornering stiffnesses are kept constant and the cornering stiffnesses values are too high for high lateral acceleration.

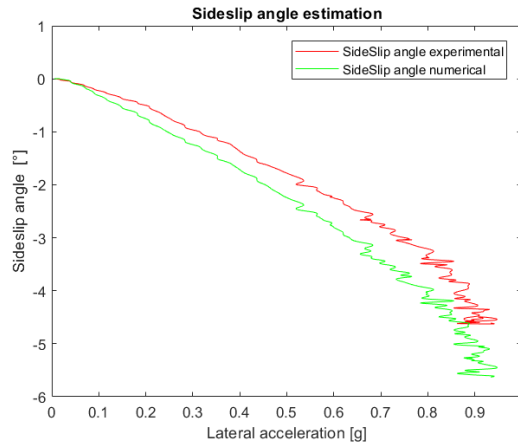


**Figure 6.9:** Sideslip angle estimation

## 6.4 Second method

The second method, as shown in the Simulink block (Fig.6.4), considers three values of cornering stiffnesses, three for the front and three for the rear. The state-space is the model showed in Eq.6.2 as in the first method. This method has been applied at the steady state reference manoeuvre, that is the ramp steer at constant nominal speed with constant steer angle rate. In this specific case a 100 km/h nominal speed and a  $20^\circ/\text{s}$  steer angle rate.

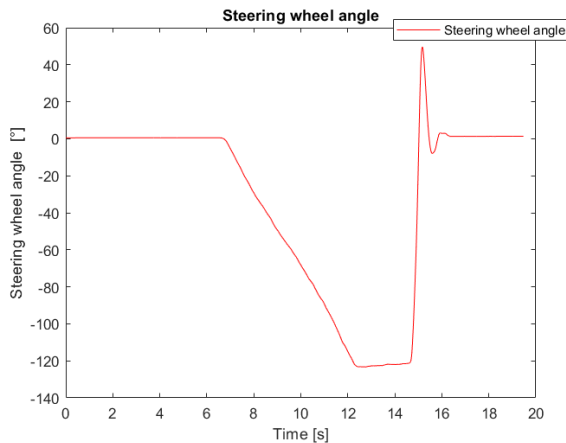


**Figure 6.10:** Steering angle

Possible cornering stiffnesses values are shown in the table.

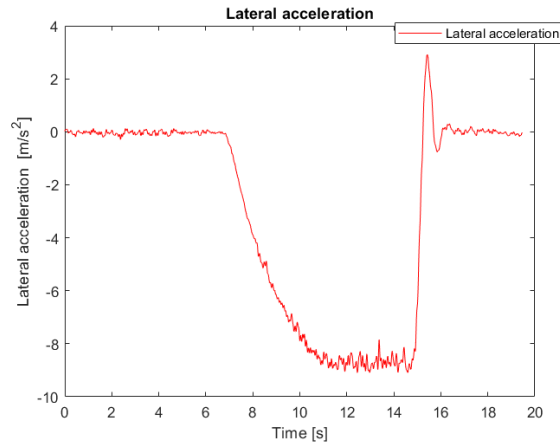


**Figure 6.11:** Lateral acceleration

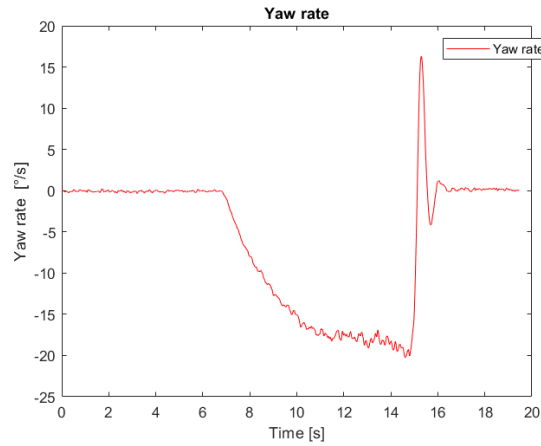


**Figure 6.12:** Yaw rate

Interval	Front	Rear
0-0.3g	120000 [N/rad]	140000 [N/rad]
0.3g-0.6g	80 000 [N/rad]	90 000 [N/rad]
0.6g-1.0g	50 000 [N/rad]	60 000 [N/rad]

The result obtained from the model shows that the gap between experimental and numerical sideslip angle can be considered constant along the manoeuvres. Furthermore, the sideslip angle estimation is improved respect to the first method, either at low and at high lateral acceleration, especially at high acceleration the

method works definitely better than the first one, fixing the problem at high acceleration.

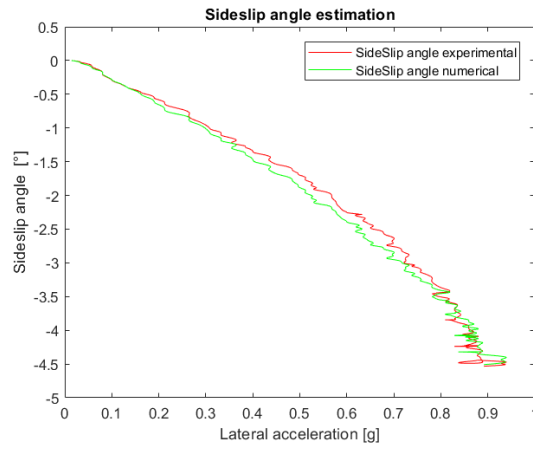


**Figure 6.13:** Sideslip angle estimation

## 6.5 Third method

### 6.5.1 Cornering stiffness estimation procedure

So far, the model worked with the assumption that the cornering stiffnesses were known. However, the cornering stiffnesses estimation, made by the FCA software, are based on the sideslip angle measurements. Therefore, the cornering stiffnesses estimation was needed. The idea behind this work was, use the kinematic model in the linear Kalman filter (Eq.2.12) to estimate the sideslip angle in steady state reference manoeuvres.

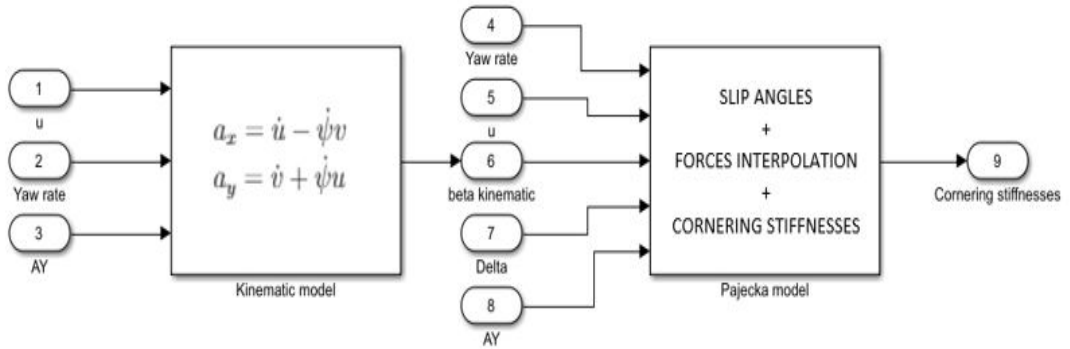


**Figure 6.14:** Simulink block cornering stiffnesses estimation

Then use the Pacejka model to compute the cornering stiffnesses and to re-enter with the cornering stiffnesses in the same model created previously, where the cornering stiffnesses were considered known. Once the cornering stiffnesses are computed in the steady state standard manoeuvres, the model can be used for every manoeuvres.

The procedure is further explained below:

1. Sideslip angle estimation with kinematic model in steady state standard manoeuvres
2. Slip angles estimation
3. Forces interpolation
4. Cornering stiffnesses estimation

Therefore, starting from the kinematic model, as already explained the system

can be represented by two equations:

$$\begin{cases} a_x = \dot{u} - \dot{\psi}v \\ a_y = \dot{v} + \dot{\psi}u \end{cases}$$

Once, the lateral speed is computed, the sideslip angle can be estimated:

$$\beta = \arctan\left(\frac{v}{u}\right)$$

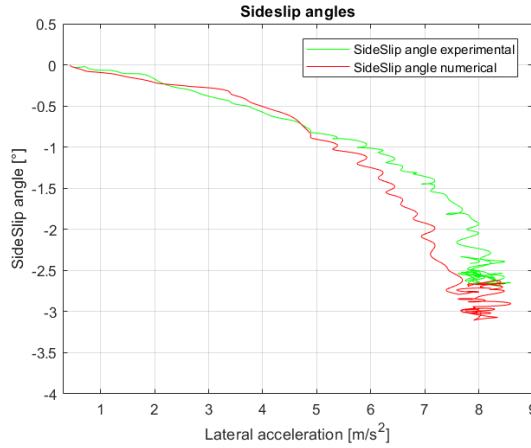


**Figure 6.15:** Sideslip angle estimation by kinematic model

The sideslip angle estimation by the kinematic model might generate several problems, especially if the signals are not with accurate off-set. In the first part an opposite sign of the angle might be estimated in some circumstances.

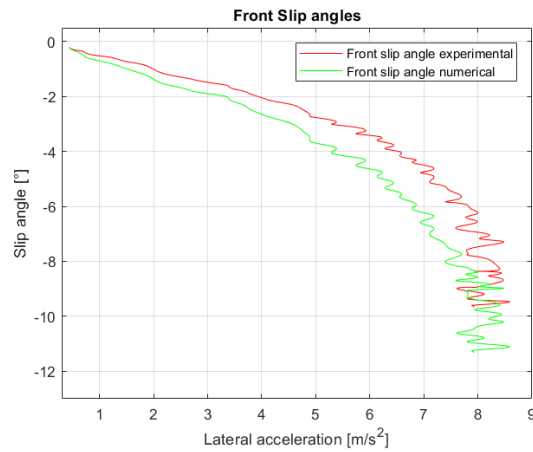
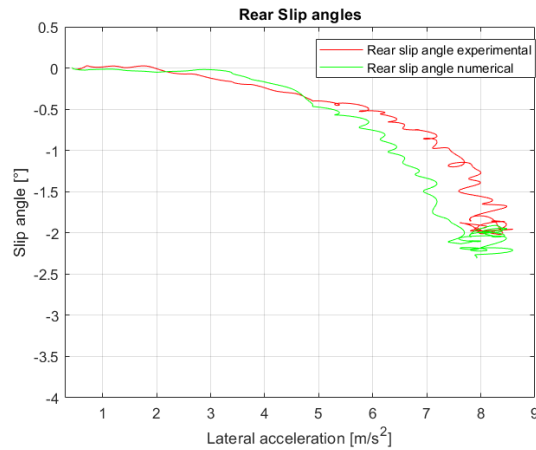
The slip angles estimation, through the equations:

$$\alpha_1 = \delta_1 - \beta + \left(\frac{\dot{\psi}}{u}\right)a_1 \quad (6.3)$$

$$\alpha_2 = -\beta + \left(\frac{\dot{\psi}}{u}\right)a_2 \quad (6.4)$$

Moreover, starting from the equilibrium equations, neglecting the longitudinal vehicle dynamic:

$$\begin{cases} ma_y = F_{y1} + F_{y2} \\ J_z \ddot{\psi} = F_{y1}a_1 - F_{y2}a_2 \end{cases} \quad (6.5)$$

**Figure 6.16:** Front slip angle estimation**Figure 6.17:** Rear slip angle estimation

It is possible to obtain the lateral forces  $F_{y1}$  and  $F_{y2}$  for the front and the rear respectively.

Remembering that this procedure is made in standard steady state manoeuvres, usually six steady state manoeuvres are used, three for each side for statistical robustness. Furthermore, forces interpolation (Fig.6.18) through the Pacejka model,

estimating the parameters B,C,D and E:

$$y(x) = D \sin(C \arctan(Bx - E(Bx - \arctan(Bx)))) \quad (6.6)$$

As explained in chapter four, the unknown parameters are computed through the *lsqcurvefit* command in Matlab. Moreover in the graph, forces at high values of slip angles are estimated, however having available data mainly up to 6° of slip angle, the reliability decreases as the curves go further this threshold, especially for the rear due to the fact that the car is an understeering vehicle and it could not usually reach these values of rear slip angle.

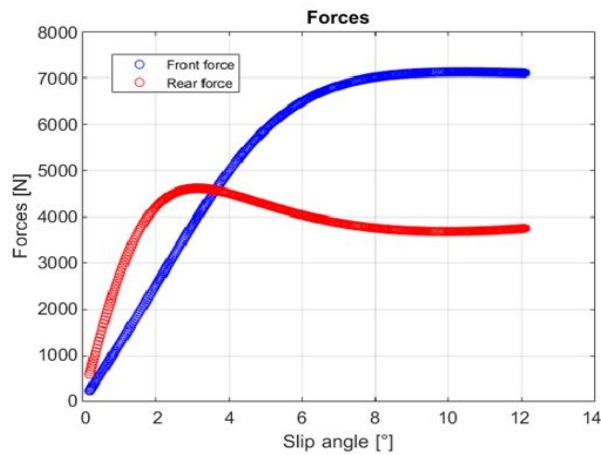


**Figure 6.18:** Front and rear forces interpolation

The resulting cornering stiffnesses estimation (Fig.6.19) are made considering the linear relation (Eq.2.5) between lateral force and cornering stiffness for each point.

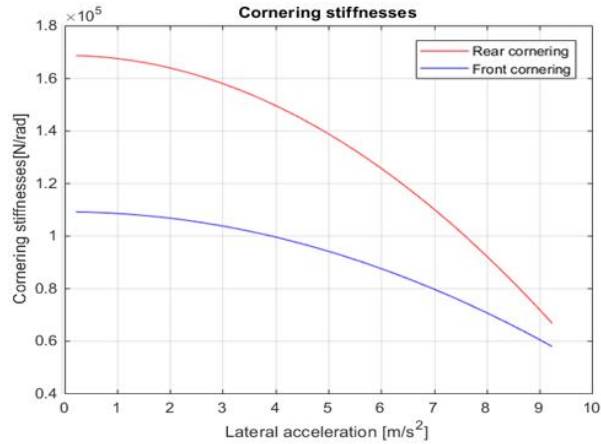


**Figure 6.19:** Front and rear cornering stiffnesses estimation

## 6.5.2 Application

In the third method, having available the entire curve of the rear and front cornering stiffnesses, at every value of lateral acceleration corresponds a value of the the cornering stiffness. In this way, the model does not need external data (Cornering stiffnesses) and it might work in several conditions of lateral acceleration even though it is based on the kinematic model estimation. Indeed the reliability of the model strongly depends on the estimation accuracy of the kinematic model.

The manoeuvres used to test the method are:

- Steady state manoeuvre
- Sweep frequency manoeuvre
- Lap at constant speed

With the steady state reference manoeuvre is immediately possible to compare the three methods accuracy. Indeed in this case it is possible to see that the estimation accuracy is lower than in the second method, due to the cornering stiffnesses estimation. Moreover the sweep frequency manoeuvre to obtain even a transient analysis, so a wider field of estimation in the vehicle dynamics. The lap is an effective circuit lap trying to keep the vehicle speed constant to neglect the vehicle longitudinal dynamic.

First, the steady state manoeuvre is tested as in the others method. The manoeuvre data are the same as in the method two, indeed only the results are shown (Fig.6.20). As it is possible to see the estimation accuracy is slightly lower than in the previous method, although the goal of this thesis is to estimate the sideslip angle in terms gap performance between tyres. A result in terms of gap performance estimation will be shown below.

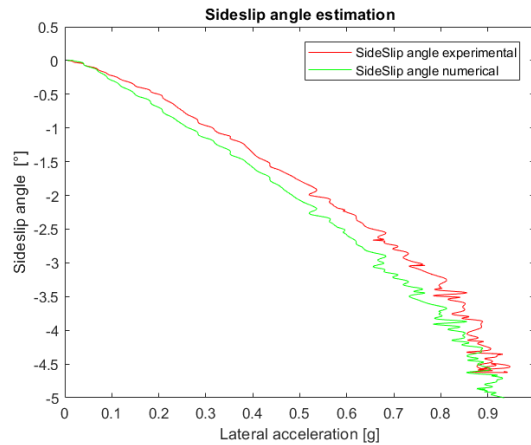


**Figure 6.20:** Sideslip angle estimation in steady state reference manoeuvre

Furthermore, the transient reference manoeuvre were used to test the model. The frequency sweep (0.7g lateral acceleration) at constant nominal speed (120 km/h) with increasing steer angle rate.

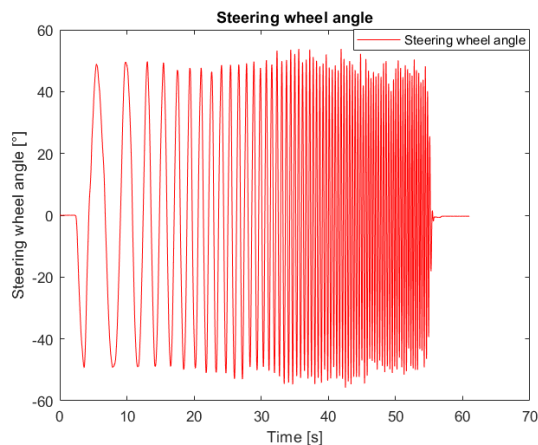


**Figure 6.21:** Steering angle in sweep frequency manoeuvre

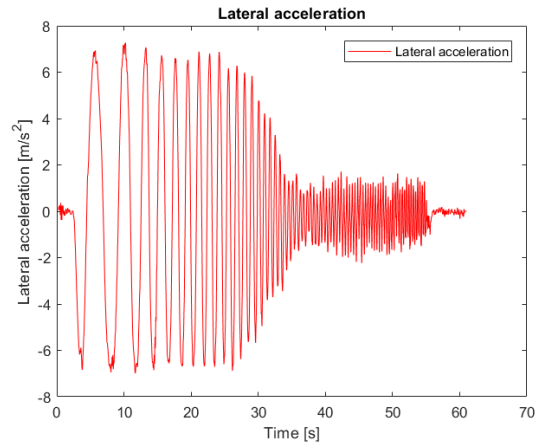


**Figure 6.22:** Lateral acceleration in sweep frequency manoeuvre

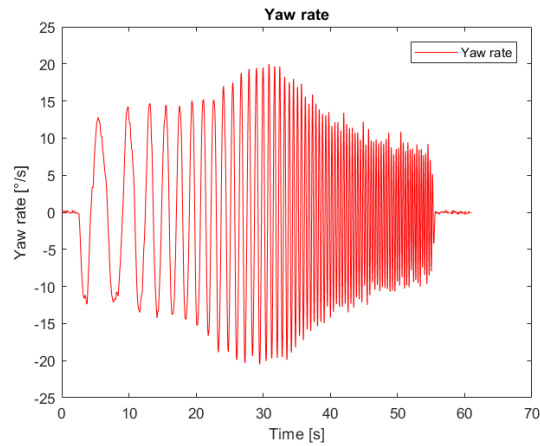


**Figure 6.23:** Yaw rate in sweep frequency manoeuvre

The result obtained from the sideslip angle estimation for the frequency sweep manoeuvre, at 0.7g lateral acceleration with estimated cornering stiffnesses, is shown in Fig.6.24 in the the Bode diagram (the sideslip angle/steering wheel angle transfer function). The results show an almost constant error along the frequencies, this is probably due to the cornering stiffnesses estimation, being the error practically constant.

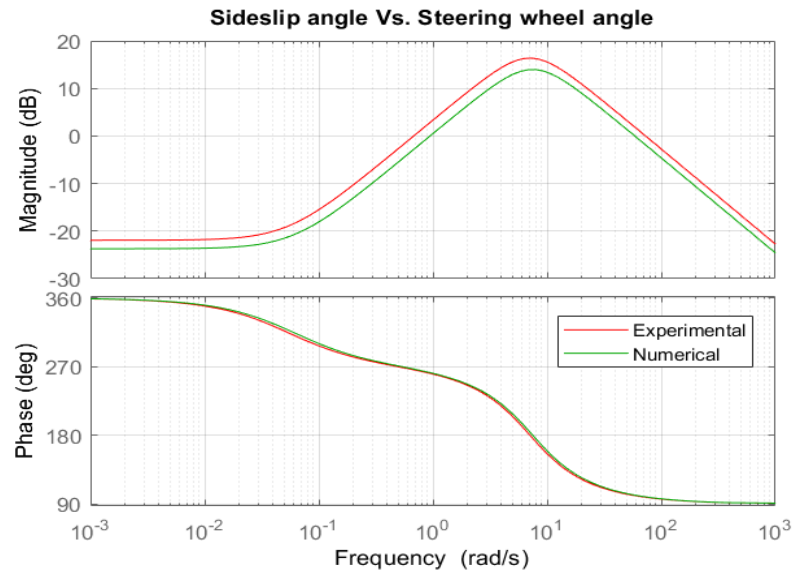


**Figure 6.24:** Bode diagram Sideslip angle estimation

Sideslip angle estimation in a lap, at almost constant speed 60 km/h in Fig(6.25):

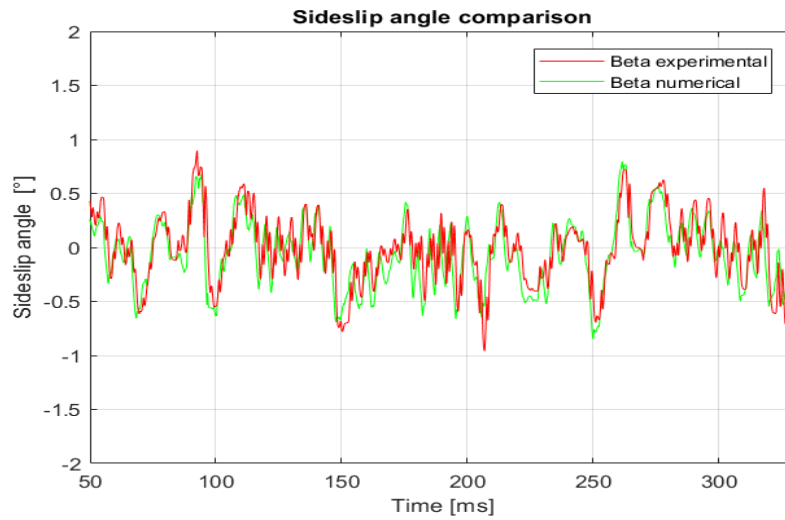


**Figure 6.25:** Sideslip angle estimation in a lap at 60 km/h

## 6.6 Error

Once the model was tested in different situations, two parameters were computed to obtain mathematical values that might be indicative for the model accuracy. Here below explained:

- The Mean absolute Error (MAE)
- The Root Mean Squared Error (RMSE)

The MAE is the average of the absolute difference between the measured value and the estimated one.

The RMSE represents the square root of the second sample moment of the differences between predicted values and observed ones or the quadratic mean of these differences.

$$MAE = \frac{1}{n} \sum_{i=1}^n |y_{measured} - y_{estimated}| \quad (6.7)$$

$$RMSE = \sqrt{\frac{1}{n} \sum_{i=1}^n (y_{measured} - y_{estimated})^2} \quad (6.8)$$

Two models of car were considered during the thesis. The type A, that is an internal combustion engine (ICE) segment C and the type B, that is an hybrid car segment C. As shown in chapter two, the theory part has been treated for front-wheel steering as the two cars considered.

For the car A, 18 types of tyres have been tested with four different rims, respectively:

- R16, three types of tyre
- R17, six types of tyre
- R18, four types of tyre
- R19, five types of tyre

For the car B, 12 types of tyres have been tested with three different rims, respectively:

- R17, five types of tyre

- R18, five types of tyre
- R19, two types of tyre

The MAE and RMSE were computed between the estimation and the experimental sideslip angle. Either for the MAE and RMSE, there are not significant differences between car A and B. Moreover the model is not affected by the rims dimension. In the table below, the MAE and RMSE are shown for the type A and B.

These two parameters are computed from the lap manoeuvre due to, first of all for the amount data available in a single manoeuvre and the practicality of making a lap instead of other standard manoeuvres. Furthermore, in a lap different conditions might be tested, in terms of lateral acceleration and sideslip angle.

CAR	MAE	RMSE
A	0.1821°	0.2124°
B	0.1917°	0.2235°

## 6.7 Sideslip angle gap comparison

The three tyres suppliers, analysed in chapter 5, are used to check the model in terms of delta sideslip angle. Moreover in Fig.6.26, the sideslip angle estimation along the lateral acceleration of the tyre 1,2 and 3 is shown. As in the chapter 5 analysis, the behaviour of the supplier 3 is the worst. Moreover, with the model used the non-linear part of the tyres is less representative due to the tyre saturation.

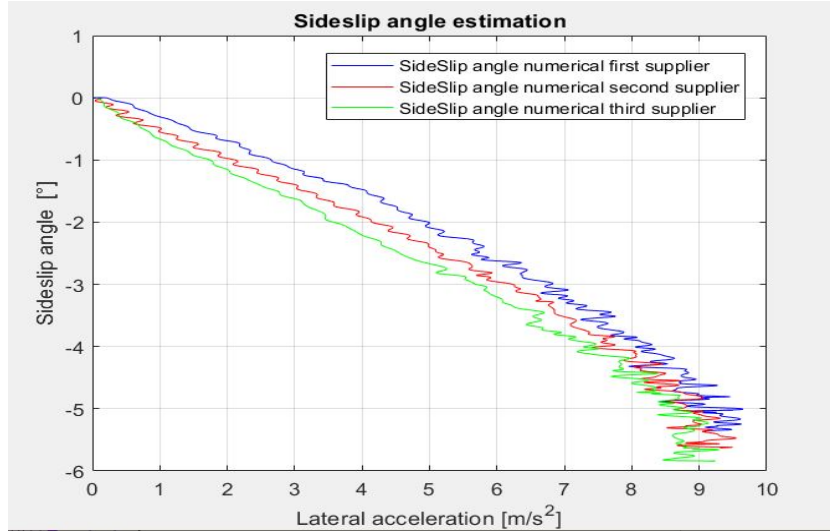


**Figure 6.26:** Sideslip angle comparison between supplier 1,2 and 3

In this way a good estimation is obtained although in chapter 5 the gap between supplier 2 and 3 is lower especially at low lateral accelerations. Anyway, the estimation represents correctly the tyres performance, showing the supplier 1 as the best and supplier 3 as the worst. This estimation is important because in testing phase, it is possible to obtain a first result about the tyres comparison performance without using the optical sensor that could be cumbersome in some situations.

## Chapter 7

# Conclusion and Outlook

This thesis has presented a combination of mathematical framework and vehicle dynamic for tyres testing performance development. The framework comprises of the vehicle's state estimation with the linear Kalman filter, combined with the Pacejka model. All three topics are linked to obtain the result as much accurate as possible.

The observer is based on the bicycle model and the linear Kalman filter method and it uses only IMU measurements. An algorithm to define the model was proposed and experimental results show that the algorithm is effective. Therefore, Kalman filter observer uses bicycle model to correct the sideslip angle estimation. The bicycle model as well as the kinematic model uses the vehicle speed instead of the longitudinal velocity which is not available due to the absence of the optical sensor.

The goals of this thesis were, first of all estimate the sideslip angle considering the cornering stiffnesses known then estimate the cornering stiffnesses and afterwards the sideslip angle. The idea behind was to use a kinematic model to first estimate the sideslip angle and then use the Pacejka model to build up the cornering stiffness curves, all done using steady state reference manoeuvres. The problem was that the kinematic model is not accurate or it might not work in a wide working-field, hence, several manoeuvres for given set-up or tyre were used to estimate the curves. In this way several data were available and the estimation was definitely closer to the experimental measurements and big mismatch were avoided.

The Sideslip angle estimation was done to compare tyres performance in testing phase. Indeed, in the third method, estimating the cornering stiffnesses, a bit of estimation accuracy was lost; although the tyres gap performance was respected and the goal achieved.

This work was done in off-line conditions, although with a first cornering stiffnesses estimation it can work even in real time, estimating the sideslip angle during the manoeuvre. This point might be also helpful in unstable vehicle condition. Indeed, This method can guarantee a prediction, thus anticipation, of unstable

behaviour.

In this thesis, only lateral dynamic was considered with additional simplification such as not considering roll rate. It could be particularly interesting also considering the longitudinal dynamic for further studies and so adapting the model at higher longitudinal speed variation.

All the key areas of this research were based on a depth analysis of the literature.



# Bibliography

- [1] Daniel Chindamo, Basilio Lenzo, and Marco Gadola. «On the vehicle sideslip angle estimation: a literature review of methods, models, and innovations». In: *applied sciences* 8.3 (2018), p. 355 (cit. on pp. 2, 3).
- [2] S Melzi and E Sabbioni. «On the vehicle sideslip angle estimation through neural networks: Numerical and experimental results». In: *Mechanical Systems and Signal Processing* 25.6 (2011), pp. 2005–2019 (cit. on p. 3).
- [3] Weida Wang, Lijuan Yuan, Sheng Tao, Wei Zhang, and Tianshu Su. «Estimation of vehicle side slip angle in nonlinear condition based on the state feedback observer». In: *2010 IEEE International Conference on Automation and Logistics*. IEEE. 2010, pp. 632–636 (cit. on p. 5).
- [4] Nenggen Ding and Saied Taheri. «A modified Dugoff tire model for combined-slip forces». In: *Tire Science and Technology* 38.3 (2010), pp. 228–244 (cit. on pp. 5, 21).
- [5] Havard Fjaer Grip, Lars Imsland, Tor A Johansen, Jens C Kalkkuhl, and Avshalom Suissa. «Vehicle sideslip estimation». In: *IEEE control systems magazine* 29.5 (2009), pp. 36–52 (cit. on p. 5).
- [6] Hassan Shraim, Mustapha Ouladsine, Leonid Fridman, and Monica Romero. «Vehicle parameter estimation and stability enhancement using sliding modes techniques». In: *International journal of vehicle design* 48.3-4 (2008), pp. 230–254 (cit. on p. 5).
- [7] JC Cadiou, A El Hadri, and F Chikhi. «Non-linear tyre forces estimation based on vehicle dynamics observation in a finite time». In: *Proceedings of the Institution of Mechanical Engineers, Part D: Journal of Automobile Engineering* 218.12 (2004), pp. 1379–1392 (cit. on p. 5).
- [8] Haiyan Zhao and Hong Chen. «Estimation of vehicle yaw rate and side slip angle using moving horizon strategy». In: *2006 6th World Congress on Intelligent Control and Automation*. Vol. 1. IEEE. 2006, pp. 1828–1832 (cit. on p. 5).

- 
- [9] Hui Zhang, Xiaoyu Huang, Junmin Wang, and Hamid Reza Karimi. «Robust energy-to-peak sideslip angle estimation with applications to ground vehicles». In: *Mechatronics* 30 (2015), pp. 338–347 (cit. on p. 5).
- [10] Seung-Han You, Jin-Oh Hahn, and Hyeongcheol Lee. «New adaptive approaches to real-time estimation of vehicle sideslip angle». In: *Control Engineering Practice* 17.12 (2009), pp. 1367–1379 (cit. on p. 5).
- [11] Jihan Ryu, Eric J Rossetter, and J Christian Gerdes. «Vehicle sideslip and roll parameter estimation using GPS». In: *Proceedings of the AVEC International Symposium on Advanced Vehicle Control*. 2002, pp. 373–380 (cit. on p. 5).
- [12] Moustapha Doumiati, Alessandro Victorino, Ali Charara, and Daniel Lechner. «A method to estimate the lateral tire force and the sideslip angle of a vehicle: Experimental validation». In: *proceedings of the 2010 American Control Conference*. IEEE. 2010, pp. 6936–6942 (cit. on p. 5).
- [13] Yupeng Huang, Chunjiang Bao, Jian Wu, and Yan Ma. «Estimation of sideslip angle based on extended Kalman filter». In: *Journal of Electrical and Computer Engineering* 2017 (2017) (cit. on p. 5).
- [14] Liang Li, Gang Jia, Xu Ran, Jian Song, and Kaihui Wu. «A variable structure extended Kalman filter for vehicle sideslip angle estimation on a low friction road». In: *Vehicle System Dynamics* 52.2 (2014), pp. 280–308 (cit. on p. 5).
- [15] Hans Pacejka. *Tire and vehicle dynamics*. Elsevier, 2005 (cit. on pp. 5, 54).
- [16] G Hodgson and Matt C Best. «A parameter identifying a Kalman filter observer for vehicle handling dynamics». In: *Proceedings of the Institution of Mechanical Engineers, Part D: Journal of Automobile Engineering* 220.8 (2006), pp. 1063–1072 (cit. on p. 5).
- [17] Guillaume Baffet, Ali Charara, and Daniel Lechner. «Estimation of vehicle sideslip, tire force and wheel cornering stiffness». In: *Control Engineering Practice* 17.11 (2009), pp. 1255–1264 (cit. on p. 5).
- [18] YF Lian, Y Zhao, LL Hu, and YT Tian. «Cornering stiffness and sideslip angle estimation based on simplified lateral dynamic models for four-in-wheel-motor-driven electric vehicles with lateral tire force information». In: *International Journal of Automotive Technology* 16.4 (2015), pp. 669–683 (cit. on p. 5).
- [19] Simon J Julier, Jeffrey K Uhlmann, and Hugh F Durrant-Whyte. «A new approach for filtering nonlinear systems». In: *Proceedings of 1995 American Control Conference-ACC'95*. Vol. 3. IEEE. 1995, pp. 1628–1632 (cit. on p. 5).
- [20] Tommaso Novi, Alex Liniger, Renzo Capitani, Marco Fainello, Giacomo Danisi, and Claudio Annicchiarico. «The influence of autonomous driving on passive vehicle dynamics». In: *SAE International Journal of Vehicle Dynamics, Stability, and NVH* 2.2018-01-0551 (2018), pp. 285–295 (cit. on p. 5).

- [21] Edouard Davin, H Henk Nijmeijer, and IJM Besselink. «Parameter identification of a linear single track vehicle model». In: *D&C* 2011 (2011) (cit. on p. 6).
- [22] Massimo Guiggiani. «The science of vehicle dynamics». In: *Pisa, Italy: Springer Netherlands* (2014) (cit. on p. 15).
- [23] Mohinder S Grewal and Angus P Andrews. *Kalman filtering: Theory and Practice with MATLAB*. John Wiley & Sons, 2014 (cit. on p. 22).
- [24] M Gadola and D Chindamo. «Estimation of vehicle side-slip angle using an artificial neural network». In: *MATEC Web of Conferences*. Vol. 166. 2001.
- [25] Manuel Acosta, Stratis Kanarachos, and Mike Blundell. «Virtual tyre force sensors: An overview of tyre model-based and tyre model-less state estimation techniques». In: *Proceedings of the Institution of Mechanical Engineers, Part D: Journal of Automobile Engineering* 232.14 (2018), pp. 1883–1930.
- [26] Mingyuan Bian, Long Chen, Yugong Luo, and Keqiang Li. *A dynamic model for tire/road friction estimation under combined longitudinal/lateral slip situation*. Tech. rep. SAE Technical Paper, 2014.
- [27] Petr PICHLÍK. «Comparison of Different Kalman Filters Types Performance for a Locomotive Slip Control Purposes». In: *Czech Technical University, Prague* (2017).
- [28] Joseph J LaViola. «A comparison of unscented and extended Kalman filtering for estimating quaternion motion». In: *Proceedings of the 2003 American Control Conference, 2003*. Vol. 3. IEEE. 2003, pp. 2435–2440.
- [29] S Konatowski, AT Pieni, et al. «A comparison of estimation accuracy by the use of KF, EKF & UKF filters». In: *WIT Transactions on modelling and simulation* 46 (2007).
- [30] Radu Drosescu and Silviu Zamfir. «MEMS based device for steering wheel angle experimental measuring». In: *Applied Engineering, Materials and Mechanics: Proceedings of the 2016 International Conference on Applied Engineering, Materials and Mechanics (ICAEMM 2016)*. World Scientific. 2016, pp. 304–313.